NEXT GENERATION BIOACTIVE GLASS DERIVED SCAFFOLD FOR BONE TISSUE ENGINEERING: SYNTHESIS AND CHARACTERIZATION

BY

SANGGU SIMON CHON

A THESIS
SUBMITTED TO THE FACULTY OF

ALFRED UNIVERSITY

IN PARTIAL FULFILLMENT OF THE REQUIREMENTS
FOR THE DEGREE OF

MASTER OF SCIENCE

IN

MATERIALS SCIENCE AND ENGINEERING

ALFRED, NEW YORK

APRIL, 2017

NEXT GENERATION BIOACTIVE GLASS DERIVED SCAFFOLD FOR BONE TISSUE ENGINEERING: SYNTHESIS AND CHARACTERIZATION

BY

SANGGU SIMON CHON

B.S. ALFRED UNIVERSITY (2014)

SIGNATURE OF AUTHOR_____

APPROVED BY_____

ANTHONY W. WREN, ADVISOR

_____

ALEXIS G. CLARE, ADVISORY COMMITTEE

_____

MATTHEW M. HALL, ADVISORY COMMITTEE

_____

CHAIR, ORAL THESIS DEFENSE

ACCEPTED BY_____

ALASTAIR N. CORMACK, INTERIM DEAN
KAZUO INAMORI SCHOOL OF ENGINEERING

ACKNOWLEDGMENTS

I would first like to express my deepest thanks to Dr. Wren for not only being a wonderful advisor to me, but also as a great mentor, whose guidance and support has allowed me to finish my work at Alfred University. I would also like to thank Dr. Hall and Dr. Clare for their presence on my thesis committee to review and criticize my work. Thank you Dr. Clare, for advising me during my undergraduate program at Alfred University and for kindly accepting to be a member of my thesis committee. Also thank you Dr. Hall, for assigning various research projects and presenting different opportunities for me to learn and experience research during undergraduate level. I want to thank my family members for their unconditional love, and supporting my goal to pursue further education. I also want to thank my friends, lab mates, and colleagues who were there for me whenever I encountered any hardship. Last but not least, I want to express my sincere gratitude to God for His presence and giving me the strength I needed as His words say, “I can do all things through Him who strengthens me” (Philippians 4:13).

TABLE OF CONTENTS

Page

LIST OF TABLES

Page

LIST OF FIGURES

Page

ABSTRACT

Substitution of TiO_2 for network modifiers (Na_2O and CaO) within a bioactive glass series was investigated to fabricate next generation bioactive glass derived scaffolds with amorphous structure and improved mechanical stability. This study consisted of initial glass characterization and mechanical durability analysis when incubated in simulated body fluid (SBF), and both synthesis and characterization of scaffolds. Three glasses were formulated for this study where a SiO_2-CaO-Na_2O-P_2O_5 bioactive glass was used as control denoted *BG*, 9 wt% substitution of TiO_2 for CaO and Na_2O were denoted *SC-1* and *SC-2*, respectively. X-ray diffraction revealed partial crystallinity in *SC-1* and *SC-2* where amorphous pattern was observed for *BG*. Differential thermal analysis indicated crystallization (devitrification) temperatures were not evident for *SC-1* and *SC-2*. Each glass was incubated in SBF for 1, 10, 100, and 1,000 hours. Scanning electron microscopy images indicated the presence of calcium phosphate deposition layer on *BG* after 1,000 hours with visible dehydration cracks. However, no visible deposition layer was observed on the surface of *SC-1* and *SC-2*. Ion release profiles of extracted SBF showed decreasing amounts of Ca and P over time, which indicated very thin layer of deposition on the surface of *SC-1* and *SC-2*. Additionally, pH measurement results on the SBF extracts of each glass after incubation study showed evidence of dissolution supported by an increase in pH where *BG* exhibited highest dissolution rate among three glasses as expected. Although the hardness of *SC-1* and *SC-2* was found to significantly decrease after each incubation period, *SC-1* and *SC-2*, when incubated for 1,000 hours presented higher mechanical durability than *BG*. Both *BG* and *SC-1* was synthesized into scaffolds *via* foam replication technique and heat treated at various temperatures. *BG* did not form a stable structure for further characterization but X-ray diffraction pattern of *SC-1* indicated low crystallinity present when heat treated at below sintering temperature. Optical stereomicroscopy showed transition of powder based material into a predominantly amorphous scaffold over the temperature region of 600 ~ 635 °C.

INTRODUCTION

1. Glass

The use of glass in today's world is very common. Its existence dates back to about five or six thousand years. The word glass is derived from a Latin word "glaesum", which means transparent material. Due to its unique aesthetic property, glass has been used in various applications since the Egyptian times. One among famous applications of glass in history was through stained glass windows used in cathedrals, which were developed during the Middle Ages [1]. In the modern world, as a result of research and exploits on the properties of glass, its application range from commercial, to advanced technology such as display panels, aerospace, and biomedical applications.

1.1. Network Structure

Shelby stated that glass can be defined as "an amorphous solid completely lacking in long range, periodic atomic structure, and exhibiting a region of glass transformation behavior" [2], essentially meaning that it can be described as a "melt quenched amorphous solid". The word amorphous is used when describing a structure that is without a clear definitive shape or form [3]. Solids such as metals and ceramics typically have a long-range order that assumes a crystal structures. However, glass is known to have a long-range disorder of network as described by Zachariasen [4]. Basic network structure of glass can easily be understood through Zachariasen's "random network theory". A representation indicating the difference between a common crystalline phase and glassy phase can be shown in Figure 1, where both forms are composed of AO_3 triangles sharing corners, however the glassy phase includes long-range disorder introduced by various bond angles of A-O-A [1].

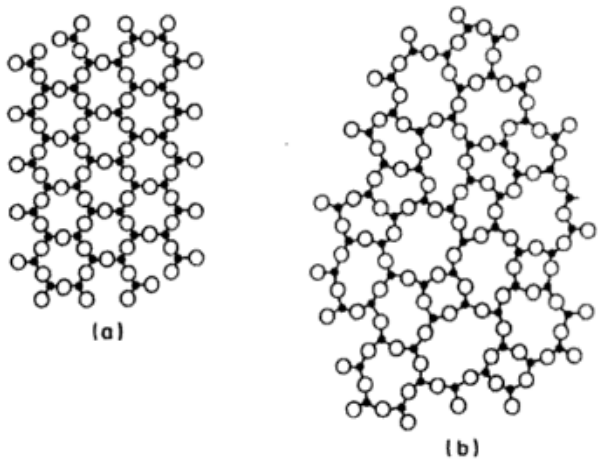

Figure 1. Crystal structure representation of (a) crysalline, and (b) glass [1].

Zachariasen stated four rules for glass formation in oxides where: first, an oxygen atom is linked to no more than two atoms of network formers, second is the coordination number of network former with oxygens are either 3 or 4, third is the sharing corners of polyhedra, and last is that at least three corners of polyhedra must be shared [1]. There are exceptions to this rule as there are different ways to form a glass network. However, it is easy to understand what glassy material is from the rules set by Zachariasen.

One of the biggest disadvantages of some glass as a material is the vulnerability to chemical attacks in fluid media [5-9]. Although technology has advanced to invent highly durable glass products from bulletproof glass to Corning Gorilla Glass®, glass is still considered brittle material. Such disadvantage was turned into an advantage when Prof. L. Hench discovered a certain silicate bioactive glass composition, which became known as Bioglass®. This composition is still used today to aid in bone tissue regeneration *via* dissolution of ions that induce formation of new bone minerals through precipitation reactions and the activity of osteoblast cells.

1.2. Glass Composition

Hench discovered Bioglass, a silicate-based glass composition that formed a bond directly to rat bone in 1969 [10,11]. This specific glass was later named Bioglass®, which is composed of $45SiO_2$-$24.5Na_2O$-$24.5CaO$-$6P_2O_5$ in weight percent. Although Bioglass® has been promising for the use of bone tissue engineering application, but many studies

were conducted to improve several disadvantages that were present. Also, attempts to increase bioactivity and cell attachment to bioactive glass, as well as bioactive glass derived scaffolds have been widely researched, which will be covered in literature review. One issue among many that is concerned with regular bioactive glass is mechanical strength when fabricated into scaffolds. Due to a less stable glass network to induce dissolution within a biological environment, the mechanical strength of such materials has been a problem that many researchers are trying to improve. Thus, the following glass system of $30SiO_2$-$28Na_2O$-$27CaO$-$15P_2O_5$ in wt% was produced as a control bioactive glass (*BG*) in this study, and 9% substitution of TiO_2 for Na_2O resulting (denoted *SC-1*). Another substitution of 9% TiO_2 was for CaO (denoted *SC-2*).

Three samples were prepared in order to study how effective TiO_2 can be in compensating disadvantages of regular bioactive glass that are currently used, and to determine which glass system can be appropriately fabricated into scaffolds for bone tissue engineering applications.

2. Titanium Inclusion

The use of titanium as one of the components of bioactive glass can be justified as titanium has been widely researched and is currently used as a bioactive material in medical devices. For instance, titanium can be processed into pure (Cp-Ti) or alloyed metals, (Ti_4Al_6V), and foams as part of the acetabular cup used in hip joint replacement as shown in Figure 2 and 3. Furthermore, titanium coating is often used as a coating material on medical implants. Piscanec et al. have studied bioactivity of TiN coating on medical implants where TiN coated hip prosthesis heads have shown spontaneous growth of calcium phosphate phases on the surface of the material [12].

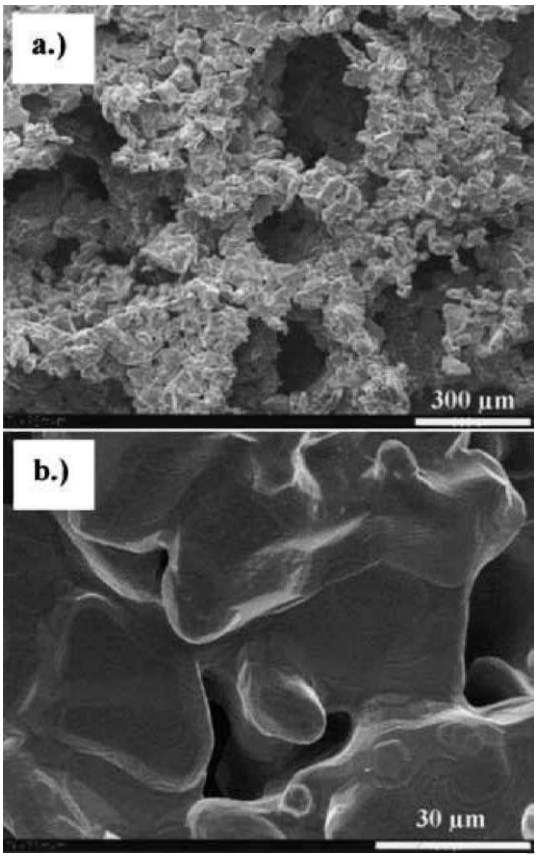

Figure 2. SEM image of porous titanium sample used in hip replacement [13].

Figure 3. Porous acetabular cup based on titanium [13].

Although only the presence of calcium phosphate phases was studied, Feng et al. have studied osteoblast adhesion of titanium surfaces containing calcium, phosphate ions

as well as carbonate apatite. Figure 4 shows osteoblast adhesion to titanium samples with different surface characteristics, and it was reported that osteoblast cells are capable of adhering onto all the samples in both flattened and elongated morphology [14].

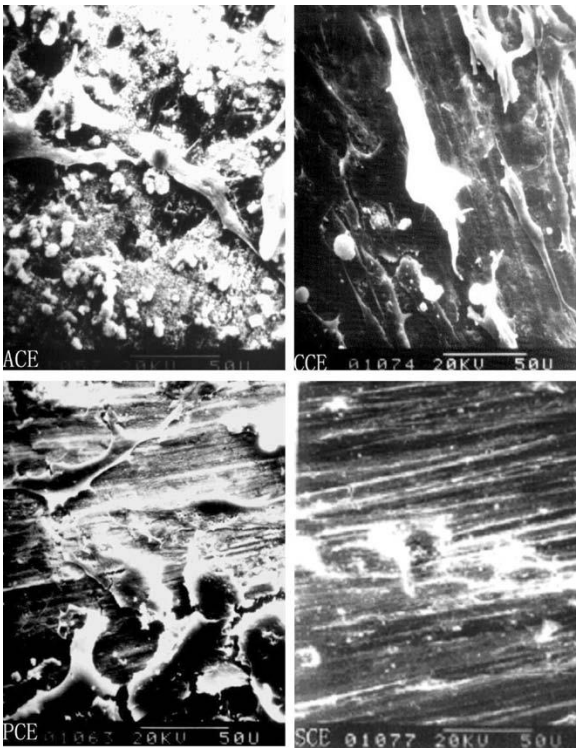

Figure 4. Osteoblast adhesion on titanium samples with different surface treatment [14].

Numerous studies conducted on titanium by many researchers suggest that titanium is considered a promising material for biomedical application due to its ability to bond directly with bone [12,14-17]. However, even such promising materials can exhibit complications in clinical applications. For instance, titanium based alloys contain partial concentrations of nickel that exhibits negative reactions within living tissues. Medical device companies to this day are focusing on how to effectively contain nickel concentrations within the devices to prevent any negative effects, such as hypersensitivity, upon implantation. Such complications are often tackled through surface treatment *via* coating or compositional changes. Similarly, bioactive glasses are currently being studied

in order to either compensate any disadvantages or to enhance bioactivity/biocompatibility.

3. Modified Glass

As mentioned above, bioactive glasses have been widely researched in order to improve their properties. Such studies include variations in fabrication method, surface engineering, and composition. Fabrication methods include both melt derived methods and sol-gel processing to determine their effect on the properties of bioactive glass [18-24]. Regardless of the fabrication method, bioactive glass interacts with living tissues of bone *via* formation of an amorphous calcium phosphate layer on the surface, which later crystallizes into hydroxyl-carbonate apatite. Such steps of what is known as "bioactivity" will be explained in detailed later. Therefore, surface engineering of bioactive glass includes inducing precipitation of hydroxyl-carbonate apatite (HCA) or amorphous calcium phosphate (ACP) particles in order to enhance bioactivity. Lastly, compositional changes in bioactive glass can include ions such as Ti^{4+}, Sr^{2+}, and Zn^{2+}, which are ions that are known to be bioactive. Current studies involve these ions being substituted for SiO_2 concentration or added within glass network. However, there have been no studies reporting substitution of TiO_2 for network modifiers with constant concentration of SiO_2 in the glass network.

3.1. Bioactivity Improvement

One of many purposes of research in bioactive glass is to improve bioactivity. Current knowledge of bioactivity of bioactive glasses was assumed to be highly dependent on the ability to form a layer that mimics the surface of bone [10,25]. However, other studies have also shown that controlled release of ionic dissolution products from degradable bioactive glasses, such as soluble Si and calcium ions, can also be the key mechanism to enhance bioactivity [10,26]. Thus, many studies have shown an increase in bioactivity through different techniques including fabrication method, compositional change, and surface engineering [24,26,27]. Furthermore, study by Salam *et al.* have reported an increase on the surface bioactivity of wallostonite glass-ceramic with the increase in the amount of Na_2O/K_2O substitution within Na_2O-K_2O-CaO-SiO_2-F glass system [26].

3.2. Amorphous vs. Crystalline

When amorphous bioactive glass is fabricated into scaffolds for bone tissue engineering application, heat treatments of the scaffold often cause crystallization of the glass. Typically, Bioglass and derivatives are heated above its crystallization temperature, which is around 610 to 630 °C, in order to produce glass-ceramic scaffolds [28-31]. It has been reported that during the crystallization phase of producing bioactive glass scaffolds, porosity is reduced due to shrinkage and the material's mechanical strength suffers [32]. However, it is noted that the low fracture toughness of such scaffolds has not yet been resolved as supporting evidences will be presented in literature review. Furthermore, a study done by Li *et al.* shows amorphous bioactive glass exhibits higher bioactivity and cell viability than crystalline bioactive glass as shown in Figure 5.

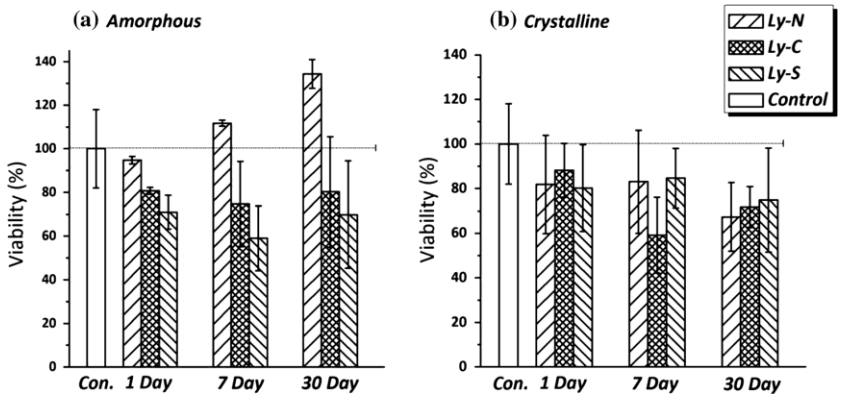

Figure 5. Cell viability comparison of amorphous and crystalline bioactive glass [33].

In other words, crystallinity may potentially increase the overall strength of the material but generally lowers bioactivity. Thus, fabricating bioactive glass based scaffolds that retain an amorphous structure can be a promising improvement in enhancing the bioactivity of the material. However, providing mechanical stability while retaining an amorphous structure for improved bioactivity still remains desirable.

3.3. Mechanical Properties

As previously mentioned, the major disadvantage of bioactive glass is poor mechanical durability. Due to its low fracture strength when fabricated into scaffolds,

bioactive glasses have not been used for load-bearing implants or replacement of joints [10,30,32]. When fabricated into scaffolds, it is difficult for the scaffolds to retain its form due to shrinkage that occurs during crystallization when heat treated, and additionally, crystallization occurs before densification of the scaffold struts that greatly compromises the mechanical integrity. Although amorphous structure increases bioactivity but it can also decrease mechanical durability where Li *et al*. had shown as represented in Figure 6 [34].

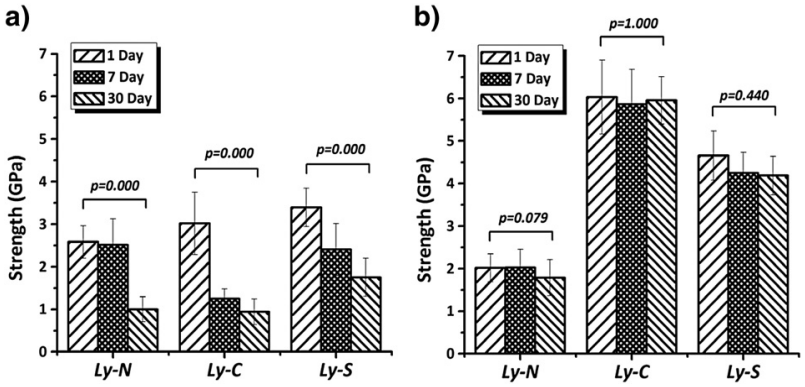

Figure 6. Hardness testing result of both amorphouse and crystalline bioactive glass samples [34].

Thus, alteration of bioactive glass composition in order to efficiently induce bioactivity through its amorphous structure and exhibit high mechanical properties are of high interest.

This study aims in the investigation of TiO_2 substitution for network modifiers within bioactive glass to determine its effect on glass structure and bioactive properties when incubated in simulated body fluid (SBF). Furthermore, characterization of fabricated scaffolds with the modified glass composition will be presented in order to achieve amorphous glass derived scaffolds with higher mechanical durability than currently known scaffolds.

LITERATURE REVIEW

1. Requirement of Medical Materials

Within several decades, it has been shown that biomaterials are materials specifically designed to repair, reconstruct, and aid regenerative properties of living tissue *via* biological activity within human body [35]. Such materials are also designed to be harmless to surrounding environment, but not all the materials are stable within the biological environment [25]. Biomaterials can generally be categorized into three different types based on their differences in biocompatibility. Categories include bioinert, bioresorbable, and bioactive materials, which are selectively discussed by Oonishi et al. [36].

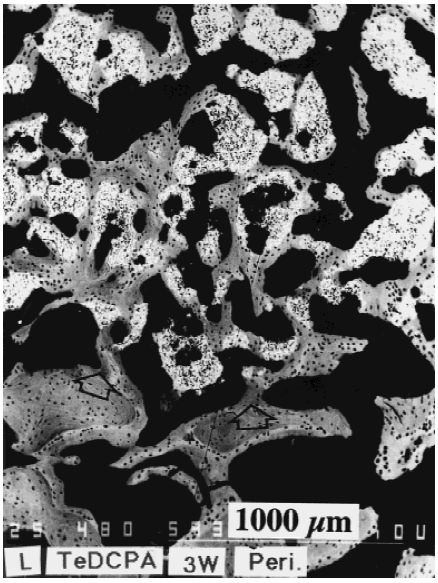

Figure 7. Back-scatter SEM image of bone growth on TeDCPA after 3 weeks [36].

There is no such thing as truly inert material within the biological environment but one of the best examples of bioinert materials are metals as interfacial bonding with living tissues generally does not occur. However, their high mechanical stability allows them to be applied as implants in biomedical applications such as knee replacements or acetabular capsules and stems for hip replacement. Another category is termed bioresorbable materials. Bioresorbable materials degrade over time when in contact with biological fluids and in some cases, through forming chemical bonds on the surface of the

materials, they are eventually replaced by healthy living tissue. Lastly, bioactive materials directly form a chemical bond with living tissues such as bone/soft tissues on the material's surface during the early stages of implantation within the host. The uses of bioinert materials such as metal implants for hip or knee replacement often require attention after the first surgery. They may act as the replacement part of the bone, but they can never transform into something similar to that of living tissue in human body. Therefore, biomaterials such as bioactive or bioresorbable materials have caught the attention of researchers and studies in order to prevent the side effects of synthetic materials upon implantation. This literature review section will discuss the background of fracture repair, bone disease and biomaterials in addition to a chronological description that explains the bioactivity of materials including bioactive glass and scaffolds.

1.1. Fracture Repair

It is well known that bone is the only tissue in our body that repairs and remodels itself through the formation of new bone instead of scar tissue. The definite process of fracture repair is still unclear as there are many factors that influence the repair process. However, the repair process can generally be broken down into four stages in both cellular and molecular events [37-39] as shown in Figure 8.

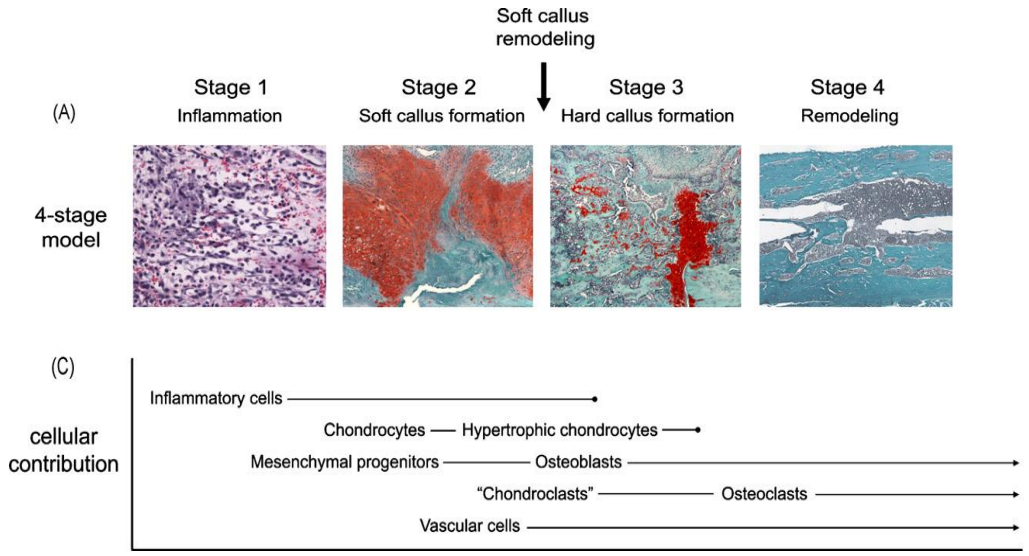

Figure 8. Fracture repair model in 4 stages with corresponding schematic of cellular contribution [40].

1.1.1. Inflammation

First stage of the process is inflammation. Upon fracture, disruption of the local soft tissues occurs as well as interruption to normal vascular function and distortion of the marrow structure [40]. When internal bleeding occurs within the fracture site, it is contained *via* a hematoma that is formed by surrounding tissues. Then, this hematoma is penetrated by multiple types of cells including, degranulating platelets, macrophages, and inflammatory cells such as granulocytes, lymphocytes, and monocytes in order to induce the following: infection resistance, secretion of cytokines and growth factors, and transformation of clotting into fibrinous thrombus [37,38]. After cellular stimulation to create capillaries, they grow into clot in order to cease internal bleeding. Lastly, macrophages and other phagocyte cells eat away left over debris and degenerated cells to proceed into next stage of fracture repair [40].

1.1.2. Soft Callus

After removal of degenerate cells, the formation of a bony callus is catalyzed by a cartilaginous template [37]. The purpose of bony callus formation is to compensate mechanical instability presented upon fracture. Chondrocytes are cells derived from mesenchymal progenitors that proliferate and synthesize cartilaginous matrix until all the fibrous tissue is replaced by cartilage [41]. Also, chondrocytes and fibroblast cells play an important role in formation of a soft callus. This soft callus does not contain any vascular forms and is considered avascular. However, a vascular system will invade later when the soft callus is developed and replaced with woven bone. This invasion by vascular endothelial cells as well as angiogenesis is stimulated *via* factors such as VEGF, BMPs, FGF-1, and TGF-β [37,42,43].

1.1.3. Hard Callus

Once soft callus development has been completed, formation of hard callus begins. This stage is where primary bone formation with the most activity of osteoblast cells occurs [37]. This activity consists of formation of new bone mineral matrix directly in the peripheral callus, essentially locations that require stability. Hard callus is typically formed near areas in need of soft callus for maintaining mechanical stability, which goes

through removal process prior to primary bone formation. However, it can also form directly to an existing surface that has been mineralized in the case of absent cartilaginous template [40]. Thus, such a four-stage model proposed here does not particularly occur in order and it is highly depended upon biological environmental condition upon fracture.

The initial woven bone is synthesized by mature osteoblasts and contains mineralized extracellular matrix tissue [40]. Also, Chen and Nakase have reported that bone morphogenetic protein (BMP) produced during the first stage play a crucial role during this process [44,45]. Additionally, other growth factors are also involved during this stage. For instance, mesenchymal stem cells incorporated within the bone marrow contributes in formation of bone during fracture repair stage [46,47]. As mentioned during third stage, invasion of vascular system occurs during this stage. The stimulation of vessel formation is highly critical during this process where hard callus is formed, because this allows increase in oxygen level in the local region for osteoblast cells to activate bone mineralization [40]. It has also been reported that this stimulation that uses angiogenic factors can supplement bone formation and fracture healing in model systems [48,49].

1.1.4. Bone Remodel

After formation of new bone with vascular integration, the final stage of bone remodeling takes place. This process involves woven bone, a hard callus into the original trabecular bone configuration where it is known as bone remodeling [40]. Although the main aspect of this stage is remodeling, it is also considered as secondary bone formation [37]. It is because the remodeling process is driven by bone resorption process and is followed by the formation of lamellar bone in an orderly fashion [40]. Bone resorption process includes activity of osteoclast cells, which are formed by differentiation and fusion of haematopoietic precursors [50]. Osteoclast cells are known as cells that eat away bone minerals. Once they are attached onto mineralized surface of bone, acid and proteinases are introduced into the surrounding, which breaks down both inorganic and organic component of the matrix. The acid environment then demineralizes, or breaks down the inorganic bone matrix and proteinases degrade collagen [40]. In a sense, bone remodeling isn't arrangement of the bone matrix but rather, reconstruction of bone

minerals via repeated degradation and formation of inorganic component by osteoclast and osteoblast cells, respectively. After demineralization of bone matrix by osteoclast cells, a pit on the bone surface known as “Howship’s lacuna” is formed where osteoblast cells are able to attach themselves on the surface and mineralize in order to reconstruct the bone matrix into correct form [40].

1.2. Bone Disease

Although human body can repair and remodel bone *via* formation of bone minerals, it is essential to have knowledge on possible causes and origins of fracture because not all fractures are eligible for self-healing process. It is common sense that one of the causes of fracture is upon accidental damage. However, individuals exhibit different limits at which bone fracture can occur. Regarding bone disease based fractures it has been reported that by 1991, an estimate of 1.5 million individuals suffer annually due to bone fracture caused by bone disease [51]. Thus, in order to fully understand what plays a role in weakening of bone, and increased fracture risk, it is important to understand the pathology of bone diseases such as osteoporosis, rickets and osteomalacia, and Paget’s disease.

1.2.1. Osteoporosis

Osteoporosis is one of the most common and well known bone diseases. The word osteoporosis represents “porous bone”. Another definition describes osteoporosis as “a skeletal disorder characterized by compromised bone strength, predisposing to an increased risk of fracture” [52]. In other words, activity of osteoclasts, which demineralize bone minerals, is higher than that of osteoblasts, which mineralize bone tissues [53].

Osteoporosis is commonly known to be present in elders. In 2001, it was reported that almost 20% individuals after the age of 50 years have developed moderate osteoporosis [54]. Such osteoporosis is categorized as primary osteoporosis. It is mainly a disease of elderly where over time, as people age, accumulation of bone loss results in deformation of bone structure [55]. This disease is considered progressive but silent that the signs and symptoms take quite some time before individuals notice them. Although it is difficult to notice early stage osteoporosis (osteopenia) without any diagnosis, several

causes of bone loss and fractures due to osteoporosis have been reported as shown in Figure 9.

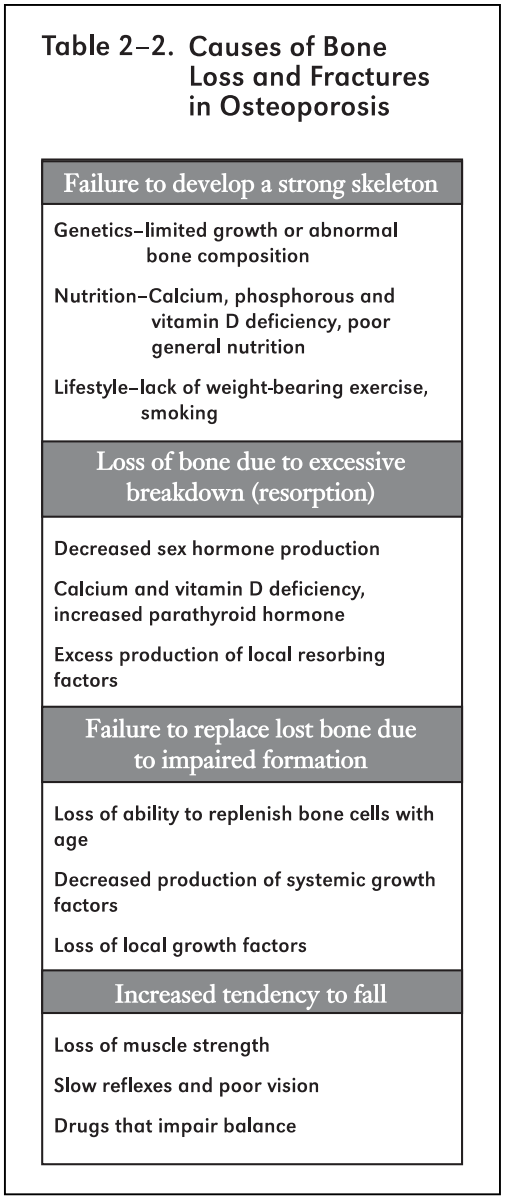

Table 2–2. Causes of Bone Loss and Fractures in Osteoporosis

Failure to develop a strong skeleton
Genetics–limited growth or abnormal bone composition
Nutrition–Calcium, phosphorous and vitamin D deficiency, poor general nutrition
Lifestyle–lack of weight-bearing exercise, smoking
Loss of bone due to excessive breakdown (resorption)
Decreased sex hormone production
Calcium and vitamin D deficiency, increased parathyroid hormone
Excess production of local resorbing factors
Failure to replace lost bone due to impaired formation
Loss of ability to replenish bone cells with age
Decreased production of systemic growth factors
Loss of local growth factors
Increased tendency to fall
Loss of muscle strength
Slow reflexes and poor vision
Drugs that impair balance

Figure 9. Causes of bone loss and fractures in osteoporosis [53].

The relationship between osteoporosis and risk of fracture can be explained by the bone density. As shown in Figure 10, bone from a patient with osteoporosis clearly shows evidence of lower bone density compared to bone from a regular healthy individual.

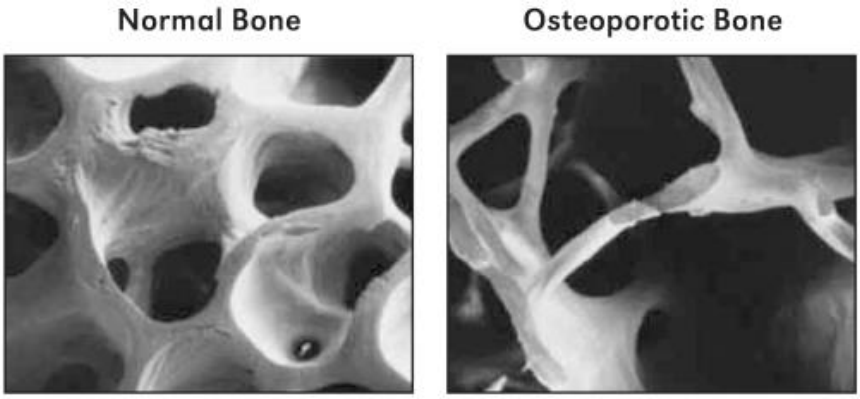

Figure 10. SEM image of trabecular bone from biopsies of normal (left) and osteoporotic (right) patients [56].

Decrease in bone density due to osteoporosis allows bone to be more vulnerable and to exhibit high risk of fracture. Additionally, frequent fractures can also lead to possibility of osteoporosis over time. For instance, in the year of 2000, it has been reported that ~9.0 million fractures advance due to osteoporosis [57].

Unlike older individuals, primary osteoporosis is rarely present on younger individuals [53]. When younger individuals are present with osteoporosis, the disease is categorized as idiopathic primary osteoporosis. This is because at such young age, exact cause of such disease is not fully understood as it includes various variables such as nutrients, genetics and environment [53]. However, Khosla *et al.* have reported that among most young adults, the disease is usually caused by factors such as anorexia nervosa or glucocorticoid use [58].

1.2.2. Rickets and Osteomalacia

Another majorly known bone diseases are rickets and osteomalacia. They both exhibit similar characteristics as bone diseases but rickets affect children and osteomalacia affects adults. As one of the causes of rickets and osteomalacia being Vitamin D deficiency, they are uncommon in the United States [53]. However, they are considered to be severe bone diseases to those who possess it [59,60]. Rickets, for children, can be caused due to low amounts of calcium phosphate mineral deposition in the growth of bone during childhood, which leads to skeletal deformation such as bowed legs [53]. On

the other hand, insufficient depositions of calcium phosphate minerals on patients with osteomalacia do not cause skeletal deformation as bone growth has stopped after childhood. However, it can increase the risk of fracture, especially in areas that have primary functions of weight-bearing such as the hip, feet, and pelvis [53]. Additionally, patients with either rickets or osteomalacia often experience muscle weakness due to lack of strength within the bone.

As previously mentioned, rickets and osteomalacia can easily be prevented with sufficient Vitamin D. Vitamin D is typically formed naturally in the skin *via* exposure to sunlight. Thus, individuals with lack of exposure to sunlight such as people living at northern latitudes have higher risk of development of this disease. For instance, Figure 11 represents an X-ray image of a certain patient's wrist that shows the evidence of rickets due to Vitamin D deficiency.

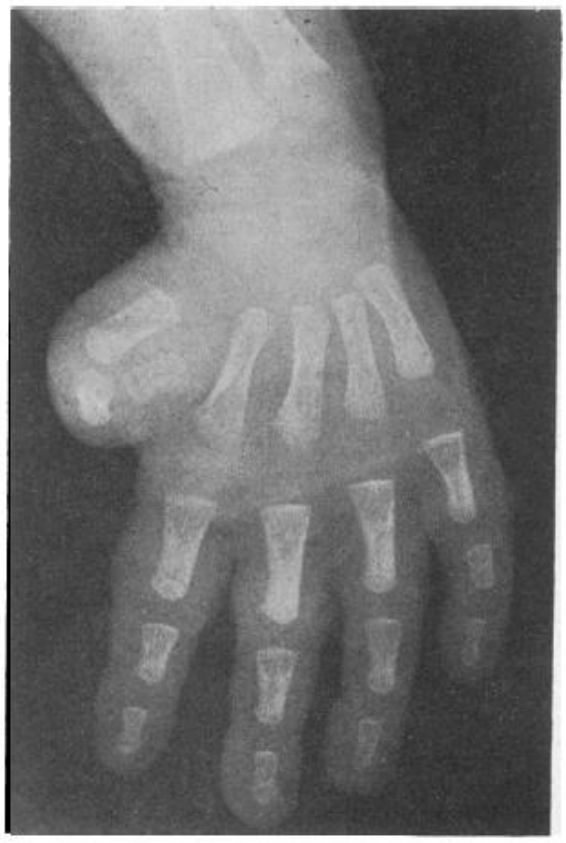

Figure 11. X-ray image of a wrist from a patient with rickets [61].

However, environmental conditions can also be one of the causes of rickets and osteomalacia and people with pigmented skin that will decrease the formation of Vitamin D are also exposed to the risk of such a disease [53]. Furthermore, another cause of rickets and osteomalacia can be genetic that can be inherited down through generations. Such genetic aspects of the disease are due to mutations of specific gene that produces an enzyme, which converts 25-hydroxy vitamin D into 1,25-dihydroxy vitamin D that is the active form, and mutation can also occur in the gene that has the primary function of developing the vitamin D receptor [62].

1.2.3. Paget's Disease

Paget's disease is a condition within the body where osteoclasts exhibit uncontrolled activity, which leads to abnormal bone resorption. Although Paget's disease is considered the second most common bone disease, accurate causes have not yet to be fully described [53]. However, it is evident that factors such as genetic mutations, environmental and viral infection can possibly explain the cause of such disease formation.

Previously, the activities and role of osteoclasts during the remodeling phase has been addressed. Paget's disease is a progressive disease that results in disorder of bone remodeling [63]. Individuals with such disease exhibit excess amount of osteoclast activity around the affected site such as spine, pelvis, legs, or even skull [53]. While such a reduction in bone density results in a deformity or increased risk of fracture, the difference between Paget's disease and osteoporosis is that the activity of osteoblasts to form bone mineral increases rapidly in order to compensate the activity of osteoclasts and it leads to a non-uniform structure. The consequences are that the volume of the bone at the affected site will increase the surrounding connective tissues and blood vessels [53]. As a result, individuals may exhibit deformed structure of bone at specific site or neurological damage caused by compression of nerve tissues.

Although many questions have not yet been answered regarding definite cause of such disorder, genetic mutation is considered one of many possible causes. For instance, 15 to 40 percent of patients with Paget's disease have reported to have at least one relative with the same disorder [64]. Furthermore, Siris *et al.* have stated that someone with

a relative that has Paget's disease is very likely to develop same disease compare to someone without any paretic patient as relatives [65]. However, it is important to note that specific types of genetic mutations to support such statements have not been answered yet as other studies have shown that viral infection with measles can also be the cause of such disorder [66].

1.3. Bone Void Filling

As knowledge of bone diseases have increased, many studies were performed in order to discover and further improve possible treatment of bone fractures that are mostly caused by bone diseases. It has been reported that 5 to 10% of patients with bone fracture run into complications due to abnormal healing of fracture site or defects present within the bone [38]. As minor bone fractures do not necessarily require total replacement of the joint, bone void filling has been widely used in clinical application to fully treat sites of fracture or sites that lack in bone mineral density. Filling of voids within bone can be done with various types of materials such as autograft, allograft, synthetic bone graft and bioactive glass. .

Various studies have reported that an ideal bone graft material should exhibit the following characteristics. First is osteointegration, which is the ability to directly form a chemical bond on the surface of the bone without any layers of living tissues in between. Second is osteoconduction, which is the ability to aid in the regeneration of bone on the surface. Third is osteoinduction, which is the ability to induce differentiation of pluripotential stem cells to an osteoblastic phenotype. Lastly is osteogenesis, which is the presence of osteoblasts activities that forms new bone mineral within the grafted material [67,68].

Autograft is considered the most effective in the application of bone void filling material because it exhibits all four characteristics mentioned above [69]. However, there are disadvantages in terms of limited availability of the material, significant consequences due to loss of blood, local sensory loss, and chronic pain [70]. It has also been reported that the amount of pain the patients experience seems to be proportional to the magnitude of surgery performance required in order to obtain such identical grafts [71]. Thus, allograft was proposed as an alternative solution due to its identical characteristics.

However, similar to autografts, various issues with allografts consisted of non-union formation of bone, which leads to fracture and possibly infection and immunogenic responses from the host tissue [72].

Figure 12. Commercial bone graft substitute products by Stryker Trauma & Extremities.

Such complications with the use of both autografts and allografts eventually lead to the development of synthetic bone graft materials. Synthetic bone grafts have shown to only exhibit two of the four characteristics to be an ideal material for bone void filling, which are osteointegration, and osteoconduction. However, it has been reported that various types of synthetic materials have been used over many years in clinical application [73]. Synthetic materials include aluminum oxide, calcium sulfate, beta tricalcium phosphate, hydroxyapatite to mimic the structure of bone, and finally bioactive glass. In order to compensate the two other characteristics that an ideal bone graft material would have, bioactive glass with components such as calcium and silicon have been widely researched.

2. Medical Glasses

Medical glasses, also known as bioactive glasses or glass-ceramics were designated with a description of "bioactive" because of their ability to induce direct bonding to living bone tissue. As many different compositions have been investigated to evaluate such bioactivity, it has been reported that some specialized compositions of bioactive glasses form a bond with soft tissues as well as hard tissues [74,75].

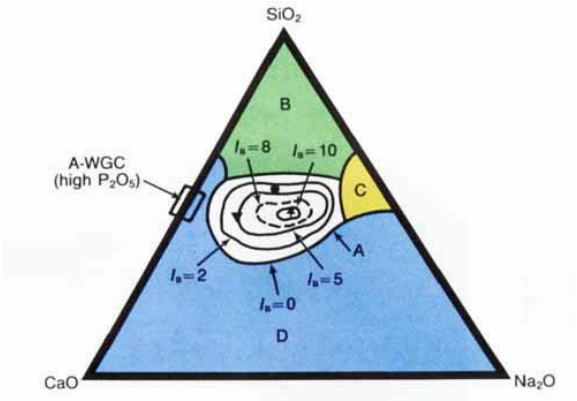

Figure 13. Compositional dependency of bioactive glass system on bond formation with living tissues [25].

Such materials that are considered "bioactive" hold certain characteristics such as time dependency of dissolution, kinetic modification of the surface upon implantation [76,77]. Many studies have been performed in order to modify medical glasses with a goal of developing better materials and it is important to understand the very first generation of bioactive glass that were developed for bone tissue engineering applications.

2.1. Bioglass

The story of bioactive glass started with a discovery by Larry L. Hench in the late 1960s. Hench proposed a hypothesis of a synthetic material that can form a hydroxyapatite (HA) structure on the material's surface to be biocompatible compared to metals or polymers that are rejected in the human body, evident by the formation of fibrous tissue [10]. This specific glass named, Bioglass®, was based on simple silicate glass

system composed of 45% SiO_2, 24.5% Na_2O and CaO, and 6% P_2O_5 in weight percentage, and it was first tested on rat femoral implants as shown in Figure 14.

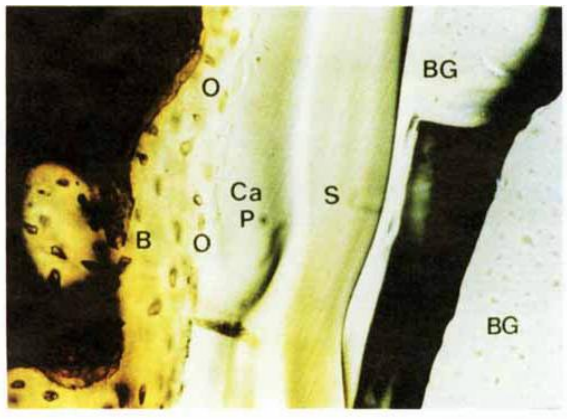

Figure 14. Optical image of direct bond of 45S5 Bioglass® implant to rat bone [78].

Although compositions of bioactive glass have a significant impact on its ability to perform bioactivity, understanding of more detailed sequences and events upon implantations were required in order to further develop advanced medical glasses.

2.2. Bioactive Response

As previously mentioned, the bioactive response associated with medical glasses involves kinetic modification on the surface of the material. Bioactivity is often described as the ability to form a direct bond with living bone tissue. However, in order to fully control the bioactivity of a material, it requires better knowledge of certain sequences that takes place within biological environment.

2.2.1. General Overview

The direct bonding of a bioactive glass to living bone tissue occurs in several steps of reaction on the surface of the glass with cell based reactions subsequently occurring. Such sequences can be categorized into seven different steps, which begin with the formation of silanol groups and the formation of a SiO_2-rich surface layer. Subsequently the adsorption of both calcium and phosphate minerals leads to the growth of an amorphous calcium phosphate layer that later crystallizes into hydroxyl-carbonate

apatite layer. Finally, osteoblast cell attachment on the surface of bioactive glass occurs. These individual steps occur chronologically where they are highly dependent on the structure, surface characteristics and biological environment.

2.2.2. Simulated Body Fluid (SBF)

Aside from clinical animal studies, synthetic fluid has been created to mimic the biological environment setting for testing material's properties in order to fully understand how biomaterials react upon implantation. For instance, simulated synovial fluid is used in medical device companies to simulate joint motion cycles to effectively determine the wear characteristics for specifically designed implant devices. In this study, simulated body fluid (SBF) was synthesized to determine bioactive reactions of bioactive glass series because it consists of various ions, with concentrations nearly equal to that of human blood plasma [79]. Furthermore, Kokubo *et al*. has reported that the ability for artificial materials to bond to living bone tissue *via* surface reaction can be reproduced with simulated body fluid [46,80].

2.2.3. Silanol Group Formation

As mentioned during the discussion of the roles of ions within a glass network, network modifiers, such as Ca^{2+} and Na^{+} ions, act as the main catalyst in the chemical reactions observed in aqueous biological environments such as SBF. Such chemical reactions are a result of dissolution of the glass surface when implanted inside the living body, where the very first phenomenon is the formation of silanol groups (Si-OH). H_3O^{+} ions from the media react with the glass causing a breakage in bonds between network formers and modifiers. Modifier ions are exchanged with H_3O^{+}, leaving OH^{-} groups to form silanol groups on the surface of the glass. Such silanol groups are then scattered across the surface of the material, which marks the beginning of the bioactivity process.

2.2.4. SiO_2-Rich Surface Layer Formation

Silanol groups that are scattered across the surface of the glass eventually lead to a continuous layer, which is achieved through polycondensation of the silanol groups [81]. The surface layer covered with continuous silanol groups become rich with SiO_2. This layer with high concentration of SiO_2, provides the setting for calcium and phosphate

ions to be chemically absorbed onto the surface from the media due to high surface area and low isoelectric point of the layer. Then through the absorption of both calcium and phosphate ions on the surface, the SiO_2 rich layer eventually becomes a crystalline HCA layer covering the entire surface of the glass [82].

2.2.5. Calcium & Phosphate Adsorption

SiO_2-rich surface layer of the glass, due to polycondensation of the silanol groups, attracts positively charged ions such as calcium and phosphate from the body fluids. This is because the continuous layer of silanol groups exhibits negatively charged units, which enhances the electrostatic interaction with ions that have positive charges [83]. Calcium ions are absorbed first onto the SiO_2-rich layer due to electrostatic interaction and phosphate ions are attracted due to positively charged calcium silicate that forms from calcium absorption. The absorption of calcium and phosphate is one of the crucial factors of bioactivity because it leads to the growth of CaP layer, which is then formed into HCA layer that will allow chemical bonding with living tissues. It is important for the aqueous environment to present enough calcium to induce calcium absorption onto the SiO_2-rich layer to attract phosphate ions to fully form a surface layer with calcium and phosphate deposition.

2.2.6. CaP Deposition Layer

As mentioned above, the calcium and phosphate absorption leads to the deposition of CaP layer on the surface of the glass above the SiO_2-rich layer. The layer is in an amorphous phase at first and grows by absorbing other ions that exist within the body fluids [84] such as Mg^{2+} and Cl^- ions [85]. The importance of this deposition is to resemble the mineral phase of bone. In other words, it is optimal for the ratio of Ca/P to reach ~ 1.65 [86]. It has been thought that such phenomena were only limited within the biological environment of living body, but not *in vitro* study such as incubation in SBF. This is because when bioactive glass has been incubated in simulated body fluid, it was expected that the calcium silicate phase on the surface continuously attracts phosphate absorption until it has been completely taken away from the aqueous media. However, several studies showed the achievement of the Ca/P ratio to reach ~ 1.65 without excess

amount of phosphate absorption on the surface of bioactive glass [87]. Moreover, Santos *et al* reported that higher formation of apatite on the surface of bioactive glass occurred with longer incubation time in SBF, but the analysis of high resolution X-ray photoelectron spectroscopy showed that the ratio of Ca/P deposition decreased with increased incubation time, possibly due to surface degradation under media over time [88]. It is evident that the absorption of calcium and phosphate plays an important role in mimicking the mineral phase of the living bone but it is not the only phenomena during this deposition. With longer incubation time, exchange of other ions occurs as well as degradation of the bioactive glass surface. For instance, the absorption of OH^- and CO_3^{2-} ions from the body fluid also occurs, which plays an important role as the catalyst in the crystallization of the amorphous deposition layer into hydroxyl-carbonate apatite layer.

2.2.7. Hydroxyl-Carbonate Apatite (HCA) Crystallization

Once an amorphous Ca/P layer on the surface of the implant exhibits Ca/P ratio similar to that of bone, the absorption of calcium and phosphate discontinues [89]. And through the initial and continuous absorption of OH^- and CO_3^{2-}, the layer crystallizes into a crystalline hydroxyl-carbonate apatite layer [84]. The crystalline HCA layer is then complete for the implanted bioactive glass to induce bioactivity through the attachment of osteoblast cells, which will then go through cellular processes to form new bone minerals. As mentioned above, certain compositions of bioactive glass can result in surface characteristic that it can form a direct bond with soft tissues such as collagen. Changes in the composition of glass will lead to differences in the bioactive response upon implantation. For instance, Figure 15 represents the bonding of HCA crystals with collagen fibrils and it has been reported that certain layer forms strong chemical bond between the bioactive glass surface and the living bone tissue for durability [90].

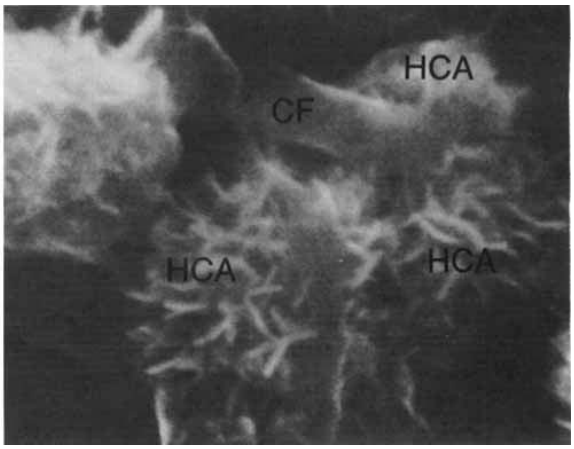

Figure 15. Bonding of HCA crystals with collagen fibril [25].

2.2.8. Osteoblast Attachment

As mentioned above, the HCA layer on the surface is crucial to induce bioactivity because the osteoblasts attach themselves on the layer to perform formation of new bone minerals. Once the osteoblasts have been attached on the surface, they will go through morphological changes in order to aid in the transportation of ions in and out of the cells *via* growth of dorsal membrane ruffles and microvilli [91]. Then the osteoblasts will continuously attach themselves on the surface to form complete cellular layers forming new bone minerals. This formation of new bone minerals is continuous process where 3-dimensional bone nodules are created to induce bone growth.

3. Scaffolds

Bioactive glasses are often used as a base material to create scaffolds, or a template structure, to enhance bone tissue regeneration and integration. Base material have not been limited only to bioactive glass as polymer based scaffolds have also been used. Furthermore, various fabrication techniques include, standard polymer foam replication method that is commonly used, starch consolidation, slip casting, freeze casting, and so on. Several studies have shown that fabrication technique results in different scaffold properties [92-94]. However, it is crucial to understand what properties of scaffold are required to be used in biomedical application.

It has been reported by various studies that an ideal scaffold for tissue engineering application exhibits the following characteristics [95-97]: (i) ability to encourage cell activities such as differentiation, delivery, attachment, and proliferation, which leads to excellent osteoconductivity that was mentioned under bone void filling literature review, (iii) controlled rate of biodegradation within biological environment, (iv) appropriate architecture and mechanical properties in order to ensure mechanical stability during formation of new tissue [98], (v) high porosity of > 90% with the range of pore diameter to be between 10 and 500 μm for easy access of cells to induce various activities such as vascularization, nutrient delivery, and waste removal [99-102]. (vi) ability to be fabricated in any type of shape to mimic structural property of targeted bone defect areas, and finally (vii) capability to scale up as commercial product, meaning the synthesis and fabrication of the scaffold must be appropriately suitable to go through sterilization and into commercialization [10].

3.1. Bioglass Derived Scaffolds

Characteristics mentioned above pertain to the case of an ideal scaffold for tissue engineering. It has been reported by several authors that bioactive glass as a base material meets the following three requirements: excellent bioactivity with osteoconductivity [11,74,103-105], controllable dissolution of ions *via* degradation [106-108], and ability to support cell activities [109]. When fabricating bioactive glass into scaffolds, the foam replication method is commonly used because the scaffolds produced with this method meet three other characteristics mentioned above: high porosity structure, flexibility in shape, and commercialization potential. Previous fabrication techniques include dry-powder processing with porogen additions [110-112], and sol-gel or gel-casting techniques [97,113]. It is important to note that 45S5 Bioglass® derived scaffolds do not satisfy the mechanical characteristic when fabricated *via* foam the replication technique and thus, modification of scaffold has gained attention among researchers.

The process consists of mixing glass powder with aqueous solution to make slurry. Polyvinyl alcohol (PVA) is added in powder form to act as a binder for fine glass particles to attach on the surface of the template foam. It is then mixed with polymeric foam where it will undergo heat treatment. The scaffold is then held above crystallization

temperature. At this stage, the polymeric template is burned off and the outcome is completely sintered bioactive glass-ceramic derived scaffold.

3.2. Current Drawbacks to Bioglass Scaffolds

According to Tancred *et al.* 45S5 Bioglass® is considered as one of the material to quickly develop hydroxyapatite layer on the surface [114]. Hence it has been commonly used to fabricate scaffolds with such glass composition. However, significant drawbacks associated with Bioglass® derived scaffolds cannot be ignored where mechanical stability is considered one of the most important issues that need improvement as mentioned above. Several studies have reported tensile strength and fracture toughness of cortical bone to be in the range of 50-151 MPa and 2-12 $MPa \cdot m^{1/2}$ and 45S5 Bioglass® showed 42 MPa and 0.7-1.1 $MPa \cdot m^{1/2}$ for tensile strength and fracture toughness, respectively [32,99]. Thus, due to low fracture toughness compared to bone, the applications of Bioglass at load-bearing sites with bone defects remain as challenge [115,116]. Furthermore, a study with fluoroapatite containing glass-ceramic scaffolds confirmed that the compressive strength values were in the range of 20-150 MPa when immersed in simulated body fluid [117] and that cortical bone is reported to have compressive strength in the range of 130-200 MPa [99,118]. It is evident that the most important disadvantage of Bioglass® derived scaffolds is its low mechanical strength.

Another drawback is uncontrolled dissolution rate, which essentially affects the cell viability. When such scaffolds are sintered at their sintering temperature to densify the glass particles, the outcome is glass-ceramic based scaffolds. It has been reported that, prior to such densification of particles, full crystallization of the glass occurs and mechanical stability is reported to be compromised [119]. Also, crystallization of bioactive glass to bioactive glass-ceramic system results in decreased cell viability [33,34].

Therefore, many studies have modified Bioglass® scaffolds *via* fabrication technique and surface engineering in order to minimize some of the significant disadvantages.

3.3. Modification Methods

Several different fabrication techniques include, but are not limited to, polymer foam replication as mentioned earlier, starch consolidation, compaction and sintering of melt-spun fibers, polymer porogen bake-out, slip casting, and freeze casting [115,117,120-123]. Different fabrication techniques will result in different structural and geometrical properties but it is also evident that such variation in techniques can influence mechanical properties as well. For instance, lamellar hydroxyapatite (HA) scaffolds fabricated by freeze casting process showed about 50 to 70% porosity and compressive strength in the range of 20 to 140 MPa, which is 2.5 to 4 times higher than conventional HA scaffolds [124]. However, scientists were faced with inevitable limitation with modification on fabrication techniques. For instance, Cannillo *et al*. have reported salt-leaching technique to create 45S5 Bioglass® derived scaffold needs further optimization to prevent precipitation as well as agglomeration of glass particles during fabrication process [125].

As a result, many researchers have studied organic polymer based coated scaffolds. Several coating studies include poly-vinyl alcohol/microfibrillated cellulose composite coating that increased compressive strength by 10 fold and tensile strength of the scaffold 20 fold [126], PHBV (poly(3-hydroxybutyrate-co-3-hydroxyvalerate)) that is biocompatible and biodegradable polymer coating on scaffolds to release vancomycin for antibacterial effect [127], and organic-inorganic hybrids containing graphene coatings to assess cell attachment on the surface [128].

Furthermore, study done by Peter *et al*. has shown that modification is not only limited to coating and different fabrication technique. Fabrication of chitosan-gelatin/bioactive glass ceramic nanoparticles *via* freezing and lyophilization technique has shown a significant effect on cell attachment compared to chitosan-gelatin scaffolds without nanoparticles as shown in Figure 16 [129]. It is interesting to note that the morphology of MG-63 cell differs significantly. Widely spread morphology of the cells on scaffolds with nanoparticles can be observed where regular GC scaffolds show more of spherical shaped cell morphology.

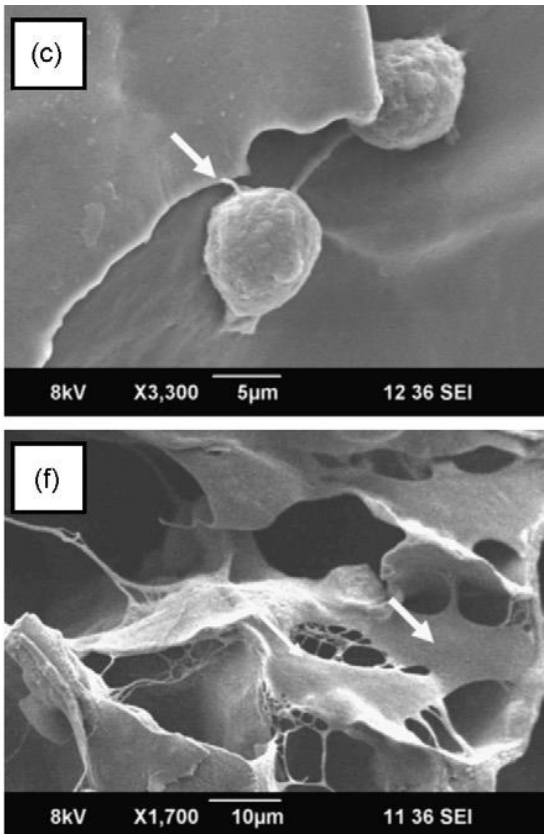

Figure 16. SEM images of MG-63 cells on GC scaffolds (c) and GC/nBGC nano-composite scaffolds [129].

It is clear to note that various modifications have been researched in order to improve currently known disadvantages of Bioglass derived scaffolds. However, obtaining mechanical stability with retained amorphous structure of scaffolds that exhibits better cell attachment/viability than currently known scaffolds have not been introduced. This study will synthesize and characterize glass composition that has been modified to substitute TiO_2 with network modifiers such as Na_2O and CaO in terms of glass structure, and measure mechanical properties when immersed under simulated body fluid for a range of hours. Then, appropriate choice of glass composition after comparison of properties will be fabricated into scaffolds *via* polymer foam replication where structural characterization and visual analysis will be noted.

With current knowledge of bioactive glass derived scaffolds, the hypothesis is that substitution of TiO_2 within glass system will increase network stability of the glass,

decrease crystallization during densification of scaffold, perform better cell attachment, and most importantly exhibit higher mechanical properties than Bioglass based scaffolds. In other words, next generation of bioactive glass derived scaffold that will retain amorphous structure with higher mechanical strength and better cell attachment.

EXPERIMENTAL PROCEDURE

1. Glass Synthesis

1.1. Glass Production

Three glass compositions (*BG*, *SC-1*, *SC-2*) were formulated for this study with the principal aim being to investigate structural changes with the substitution of TiO_2 for the network modifiers (CaO and Na_2O) within bioactive glass as shown in Table I. A control bioactive glass (*BG*), which did not contain TiO_2, was used as control. Glasses were prepared by weighing out appropriate amounts of analytical grade reagents (Sigma-Aldrich, Dublin, Ireland) and ball milling for 1 hour.

Table I. Glass Composition (wt %)

Sample	SiO_2	Na_2O	TiO_2	CaO	P_2O_5
BG	30	28	-	27	15
SC-1	30	29	9.0	16	16
SC-2	30	17	9.0	28	16

1.2. Glass Powder Production

The powdered mixes were fired at 1500°C for 1 hour in platinum crucibles and shock quenched in water. The resulting frits were dried, ground and sieved to retrieve glass powders with a maximum particle size of 90μm.

2. Material Characterization

2.1. X-ray Diffraction (XRD)

Diffraction patterns were collected using a Siemens D5000 X-ray Diffraction Unit (Bruker AXS Inc., WI, USA). Glass powder samples were packed into standard stainless

steel sample holders. A generator voltage of 40kV and a tube current of 30mA were employed. Diffractograms were collected in the range $10^{\circ}<2\theta<80^{\circ}$, at a scan step size 0.02° and a step time of 10s. Any crystalline phases present were identified using JCPDS (Joint Committee for Powder Diffraction Studies) standard diffraction patterns.

2.2. X-ray Photoelectron Spectroscopy (XPS)

X-ray Photoelectron Spectroscopy was performed in a Kratos AXIS 165 spectrometer (Kratos Analytical, Manchester, UK) using monochromatic Al Kα radiation ($h\upsilon$ =1486.6 eV). Glass rods with dimensions of 15×3×3mm were produced from the melt and fractured under vacuum (~ 2×10^{-8} torr) to create pristine surfaces with minimum contamination. Surface charging was minimised by flooding the surface with low energy electrons. The C 1s peak of adventitious carbon at 284.8 eV was used as a charge reference to calibrate the binding energies.

2.3. Particle Size Analysis (PSA)

Particle size analysis was conducted using a Beckman Coulter Multisizer 4 Particle size analyzer (Beckman Coulter, Fullerton, C.A, USA). The glass powder samples (where n=3 per glass) were evaluated in the range of 0.4 μm - 100.0 μm and the run length took 60 s. NaCl solution was used as solvent and testing was conducted at standard laboratory temperature range, 25°C. The relevant volume statistics were calculated on each glass.

2.4. Scanning Electron Microscopy/Energy Dispersive Spectroscopy

Sample imaging was carried out with an FEI Co. Quanta 200F Environmental Scanning Electron Microscope equipped with an EDAX Genesis Energy-Dispersive Spectrometer. Secondary electron (SE) and backscattered electron (BSE) images were taken on glass particles.

2.5. Differential Thermal Analysis (DTA)

A combined differential thermal analyser-thermal gravimetric analyser (DTA-TGA) (Stanton Redcroft STA 1640, Rheometric Scientific, Epsom, UK) was used to measure the glass transition temperature (T_g) for all glasses. A heating rate of $10^{o}C\ min^{-1}$

was employed using an alumina crucible where a matched alumina crucible was used as a reference. Sample measurements were carried out every six seconds between 30˚C and 1300˚C.

2.6. Hot Stage Microscopy (HSM)

A MISURA side view hot stage microscope (HSM), Expert Systems, (Modena, Italy), with image analysis system and electrical furnace, with max temperature of 1600˚C and max rate of 80˚C/min. The parameters for this experiment were a heat rate of 20˚C/min from 20˚C to 1200˚C. The computerized image analysis system automatically records and analyses the sample geometry during heating.

2.7. Magic Angle Spinning Nuclear Magnetic Resonance (MAS-NMR)

Si^{29} magic angle spinning (MAS) nuclear magnetic resonance (NMR) studies were performed using a Bruker Avance NMR spectrometer (Bruker Corp., MA, USA). A 9.4 T magnet was utilized (400.24 MHz proton Lamor frequency, 79.51 MHz 29Si Lamor frequency), using a probe head for 7 mm rotor diameters. The small powder samples (<90 μm (were spun at 5 kHz, and 200 scans were performed with a single pulse excitation (80° pulse length, 28 kHz rf field strength). The recycle delays were chosen to be three times the spin lattice relaxation times, which were determined through inversion recovery sequences to be between 15s and 26s. The chemical shift scale was externally referenced against kaolin as a secondary chemical shift standard at -91.34 ppm (center between doublet).

3. Sample Preparation of Incubation Media

3.1. Sample Preparation

Disc samples (*BG, SC-1, SC-2*) were prepared by weighing approximately 0.5 g glass powder into a stainless-steel die (sample dimensions 1.5 × 6/ mm) which was pressed under 3 tons of pressure. Disc samples were kept amorphous by heat treating the pressed discs below the glass transition temperature for 24 h. Discs of each glass were autoclaved prior to use and Simulated Body Fluid was used as the solvent to prepare extracts. The volume of extract was determined using equation 1.

$$Vs = \frac{Sa}{10} \quad (1)$$

Vs = volume of extract used.
Sa = exposed surface area of the disc.

3.2. Simulated Body Fluid Preparation

Simulated body fluid (SBF) was produced in accordance with the procedure outlined by Kokubo *et al* [80]. The composition of SBF is outlined in table 2. The reagents were dissolved in order, from reagent 1–9, in 500 ml of purified water using a magnetic stirrer. The solution was maintained at 36.5 ˚C. 1 M-HCl was titrated to adjust the pH of the SBF to 7.4. Purified water was then used to adjust the volume of the solution up to 1L. Discs (*n = 3*) were immersed in concentrations of SBF as determined by equation 1 and were subsequently stored in for 1, 10, 100, 1,000 hours in an incubator at 37˚C. A JOEL JSM-840 scanning electron microscope equipped with a Princeton Gamma Tech (PGT) Energy Dispersive X-ray (EDX) system was used to obtain secondary electron images and carry out chemical analysis of the surface of disc pellets. All EDX spectra were collected at 20 kV, using a beam current of 0.26 nA. Quantitative EDX converted the collected spectra into concentration data by using standard reference spectra obtained from pure elements under similar operating parameters.

Table II. Ionic composition of SBF

Order	Reagent	Amount
1	NaCl	7.996 g
2	$NaHCO_3$	0.350 g
3	KCl	0.224 g
4	$K_2HPO_4 \cdot 3H_2O$	0.228 g
5	$MgCl_2 \cdot 6H_2O$	0.305 g
6	1M-HCl	39 ml
7	$CaCl_2$	0.278 g
8	Na_2SO_4	0.071 g
9	$NH_2C(CH_2OH)_3$	6.057 g

4. Glass Solubility Analysis

4.1. Inductively Coupled Plasma-Optical Emission Spectroscopy (ICP-OES)

Each disc (*BG*, *SC-1* and *SC-2*, where n = 3) was immersed in simulated body fluid (SBF) for 1, 10, 100, 1,000 hours. Each disc (1.5 × 6 mm) was submerged in ~6 ml of SBF and incubated at 37 °C. The ion release profile of each specimen was measured using inductively coupled plasma-atomic emission spectroscopy (ICP-AES) on a Perkin-Elmer Optima 5300UV (Perkin Elmer, MA, USA). ICP-AES calibration standards were prepared from a stock solution on a gravimetric basis and SBF solution with different ionic composition as listed in Table 2 was used as control.

4.2. pH Analysis

Changes in the pH of solutions were monitored using a Corning 430 pH meter. Prior to testing, the pH meter was calibrated using pH buffer solution of 4.00 ± 0.02 and 7.00 ± 0.02 (Fisher Scientific, Pittsburg, PA). Sample solutions were prepared as simulated body fluid extracts by exposing disc samples (n =3) in calculated quantities of simulated body fluid. Measurements were recorded at 1, 10, 100, and 1,000 hours.

5. Mechanical Evaluation

5.1. Hardness Testing

Hardness testing was completed on glass discs mounted in epoxy resin after 1, 10, 100, 1,000 hours' incubation in simulated body fluid. A total of 10 measurements were taken on each glass plate and 3 regions on each glass disc were analyzed (*total n=30/sample*). A Shimadzu HMV-2000 Hardness testing machine was used with a 500g-load cell with 10s intervals.

6. Scaffold Synthesis

6.1. Synthesis Method

Scaffolds were produced with glass formula assigned as *SC-1*, where *SC-1* contains TiO_2. Polyvinyl alcohol (PVA, 0.002 g) was initially dissolved in 0.5 ml of de-ionized water heated until all the PVA particles were dissolved. 1 g of glass powder was gradually added to each flask and stirred until change in viscosity was observed. 10 mm x 8mmϕ rectangular polyurethane foams were cut and immersed in the glass slurry. Foams were then stirred until the pores were fully filled with the slurry. Then, immersed foams were squeezed using hand to prevent any clustering of glass slurry within the foams. The scaffolds were then heat treated in a furnace up to 400 °C at a rate of 1 °C/min to burn out polyurethane foam and further heat treated up to temperatures of 600, 610, 620, and 635°C at a rate of 1 °C/min. Scaffolds were then held at each temperature for 5 hrs.

7. Scaffold Characterization

7.1. X-ray Diffraction

Diffraction patterns were collected using a Siemens D5000 X-ray Diffraction Unit (Bruker AXS Inc., WI, USA). Scaffolds were grounded into powder samples, which were packed into standard stainless steel sample holders. A generator voltage of 40kV and a tube current of 30mA were employed. Diffractograms were collected in the range $10^{\circ}<2\theta<80^{\circ}$, at a scan step size 0.02° and a step time of 10s. Any crystalline phases present were identified using JCPDS (Joint Committee for Powder Diffraction Studies) standard diffraction patterns.

7.2. Optical Stereomicroscopy

Optical imaging was conducted on a Lecia M165 FC Optical Stereomicroscope equipped with fluorescent capabilities. Images were taken at 12.0X magnification and captures with LAS V4.8 imaging software.

RESULTS AND DISCUSSION

1. Effect of Ti^{4+} on SiO_2-CaO-Na_2O-P_2O_5 Glass Structure

1.1. X-ray Diffraction (XRD)

Several characterization techniques were performed to confirm the structure and batch compositions of the starting glasses, as listed in Table I, as well as thermal properties. Initial characterization was conducted to determine crystallinity of the glass powder after synthesis where Figure 17 represents X-ray diffraction (XRD) patterns obtained for all glasses. *BG* showed amorphous XRD pattern while *SC-1* showed an amorphous structure with minor traces of crystallinity while the crystalline phases presented in *SC-2* were identified as $Na_2Ca_4(PO_4)_2SiO_4$, Sodium Calcium Phosphate (Ref. 00-033-1229) by JCPDS software. Although a shock quench method was used to produce all glasses, crystalline phase of sodium calcium phosphate silicate present in *SC-2* indicates titanium may be acting as nucleating agent within this glass.

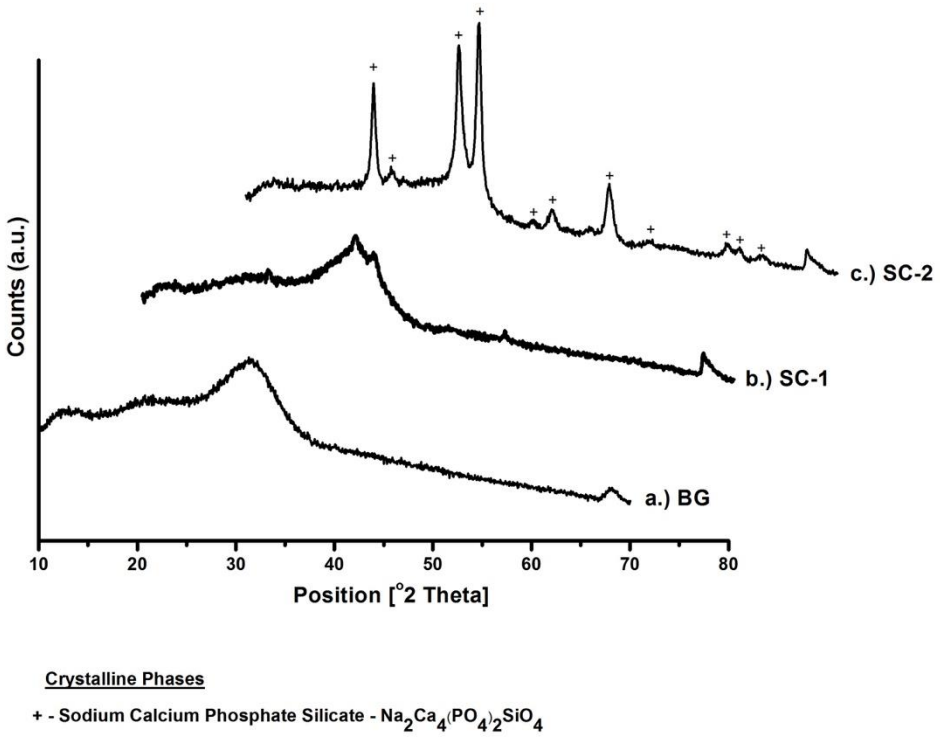

Figure 17. X-ray diffraction patterns of control and Ti containing glass series.

1.2. X-ray Photoelectron Spectroscopy (XPS)

Compositional analysis of each glass was then determined using X-ray photoelectron spectroscopy (XPS) as shown in Figure 18, which represents the survey scan of *BG* that contains Na, O, Ca, P, and Si with minor traces of carbon (C). Both *SC-1* and *SC-2* show presence of Na, O, Ti, Ca, P, and Si with minor traces of carbon (C) as well, which corresponds with initial glass batch composition as shown in Table I.

X-ray photoelectron spectroscopy (XPS) was used to confirm the glass compositions and to find any possible contamination within the samples. Figure 18 represents XPS survey scan of all three glasses where elements present in the scan correspond to the initial glass batch composition showing there was no contamination within the samples. For instance, observation of Ti^{4+} presence can be made in *SC-1* and *SC-2* but not in *BG* as shown in Figure 18. Another observation can be made to the difference in the intensities of Na^{+} detected by XPS in *SC-1*. This can be explained by the Na^{+} being a mobile ion, which tends to migrate to fracture/exposed surfaces on glass.

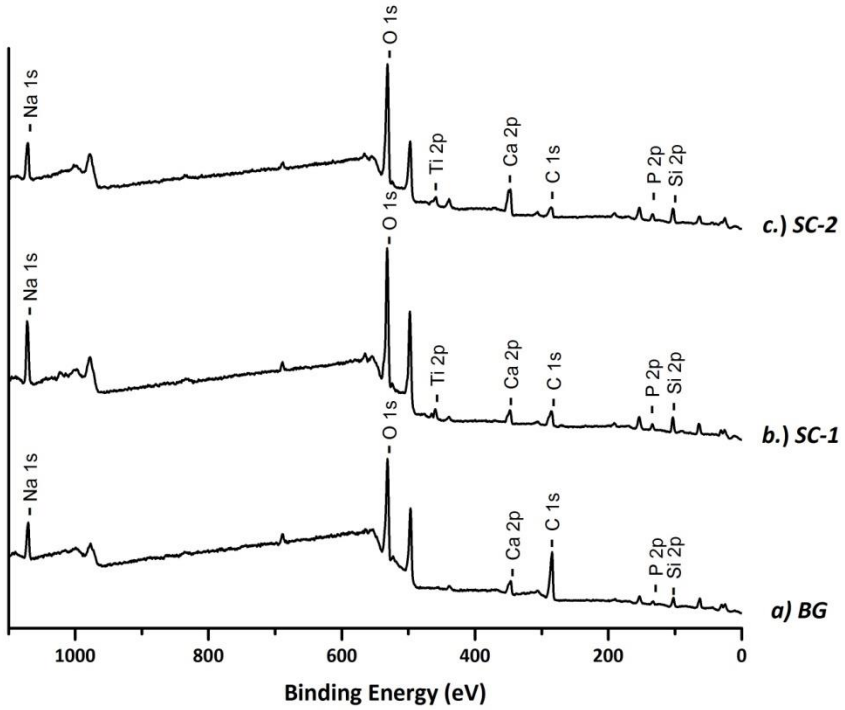

Figure 18. X-ray photoelectron spectroscopy survey scans of all three glasses.

1.3. Particle Size Analysis (PSA)

Particle size analysis was used to determine mean particle size of all glasses, which was obtained to be 12.11, 11.79, and 11.07 μm for *BG*, *SC-1*, and *SC-2*, respectively. Standard deviation with d10, d50, and d90 values were determined as well using PSA for all three glasses as shown in Table III.

It is evident that the mean particle size between three glasses was consistent with a range of 11 to 12 μm. Particle size of glass powder plays an important role when studied under fluid media because it predominates surface area characteristics of pellets, which influences the surface reactivity of glasses. For instance, study done by Arcos *et al.* have shown that various SiO2-CaO-P2O5 glass systems, produced by sol-gel method, that exhibits different surface area show difference in ionic release of ions where it is noted that glasses with surface area of 173 ± 2 m^2/g show no significant difference in ionic release but glass with much lower surface area (88 m^2/g) exhibits significant change in the ion release profile [130]. Furthermore, the effect of particle size on ion release has been an important factor when testing the antibacterial effect of bioactive glasses. Waltimo et al. have shown that bioactive glass with nano-particles displayed higher antibacterial effects due to higher release of alkaline species compared to glass with micron-sized particles [131].

Thus, it is important to note that all three glasses produced in this study show no significant difference in particle size distributions and safe assumptions can be made that any significant change in ion release profile is not influenced by differences in the mean particle sizes.

Table III. Particle Size Distribution of Glass Series

Sample	Mean (μm)	S.D. (μm)	d_{10} (μm)	d_{50} (μm)	d_{90} (μm)
BG	12.11	8.60	6.51	9.13	20.87
SC-1	11.79	8.09	6.48	9.03	19.95
SC-2	11.07	6.98	6.44	8.73	18.15

1.4. Scanning Electron Microscopy/Energy Dispersive Spectroscopy (SEM/EDS)

After synthesis, additional characterization on three glass compositions included scanning electron microscopy (SEM) for imaging, and energy dispersive spectroscopy (EDS) for semi-quantitative chemical analysis of particles as shown in Figure 19.

Back scattered electron (BSE) images of glass samples in powder form and corresponding EDS analysis match with the initial batch composition as shown in Figure 19. Also, it is noted that the element presented in EDS spectrum correlates with the XPS survey scan of all samples as shown in Figure 18. This also supports that no contamination was present during the synthesis of glasses *via* melt derived technique.

The morphology of the particles were irregular shaped but all three glasses exhibited similar morphologies where range of particle size can be seen up to 300~400 μm. The morphology of the particles showed similar findings as a study done by Vogel *et al.* where particles from different Bioglass® compositions (45S5, 52S, and 55S) were used for animal testing *via* implantation in rabbit models [132].

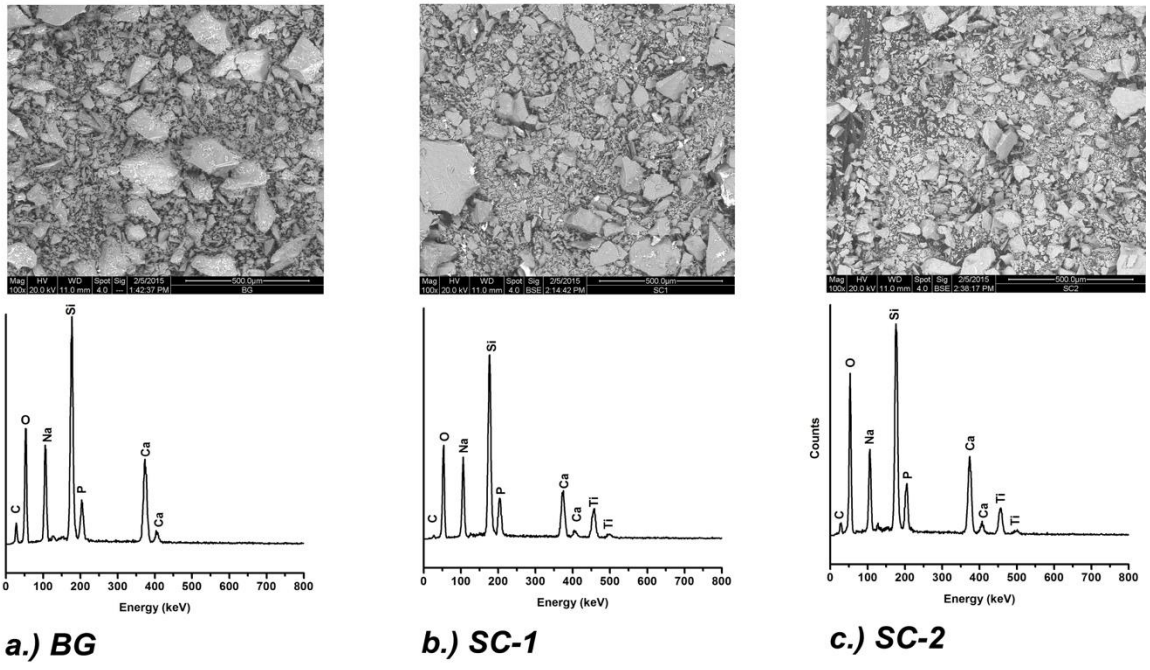

Figure 19. Scanning electron microscopy and EDS analysis on glass particle series.

1.5. Differential Thermal Analysis (DTA)

Differential thermal analysis showed glass transition temperature (T_g) and thermal history of all glasses as shown in Figure 20. Increase in T_g from 532°C (*BG*) to 559°C (*SC-1*) and to 627°C (*SC-2*) can be observed when Ti was substituted with Ca and Na, respectively. It also shows the absence of crystalline peaks of *SC-1* and *SC-2* glasses during heating.

T_g increased from 531°C to 559°C when TiO_2 was substituted for CaO and to 627^{o}C for Na_2O. This indicates the increase in stability of glass network when Ti^{4+} is introduced into the glass network. This increase in T_g can also be seen in a study where decrease in defect concentration of glass can be seen with respect to increase in the long-range order of the network when Ti^{4+} is introduced [133], Ti^{4+} may act as an intermediate interacting with both network formers and modifiers. Unlike previous studies where Ti^{4+} was substituted with network formers such as Si^{4+} result in the decrease of T_g [134], observations can be made that the substitution of Ti^{4+} for network modifiers such as Ca^{2+} and Na^{+} results in an increase of the glass network stability. Also, absence of exothermal reaction for *SC-1* and *SC-2* corresponds with crystalline phase present in the XRD pattern from Figure 17, which also led to possibility of fabricating amorphous scaffolds.

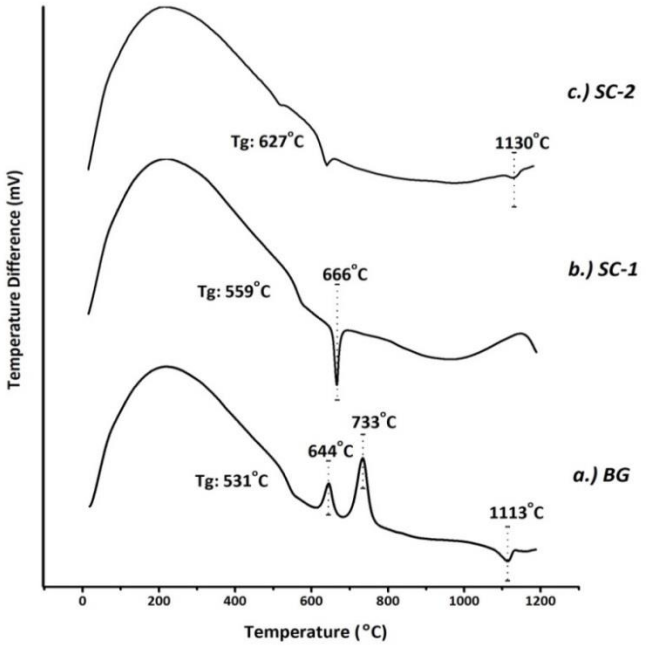

Figure 20. Differential thermal analysis of glass series.

1.6. Hot Stage Microscopy (HSM)

Additionally, hot stage microscopy was performed to determine sintering (T_s), softening (T_f), and melting (T_m) temperatures of *BG*, *SC-1*, and *SC-2* as shown in Figure 21. *SC-2* can be observed with the highest T_s, T_f, and T_m among three glasses while *SC-1* shows lowest T_s and T_m in comparison. Three temperature points were determined based on the shape of prepared sample by the instrument.

It is evident that the substitution of Ti^{4+} for different network modifiers can have different impact on the thermal properties of bioactive glasses. The sintering temperature (T_s) of *BG* was found to be at 634 ^oC. However, with the substitution of Ti^{4+} for Ca^{2+}, the T_s increased to 671 ^oC and to 761 ^oC when substituted for Na^+. The softening temperature (T_f) of both *SC-1* and *SC-2* with the substitution of Ti^{4+} showed increase from 944 ^oC to 979 ^oC and 1150 ^oC, respectively. However, melting temperature (T_m) showed different result. The T_m of *SC-1* was lower than that of *BG*, 1104 ^oC and 1135 ^oC, respectively. Such sintering temperatures of each glasses were indicated as the temperature range at which densification will occur during synthesis of scaffolds.

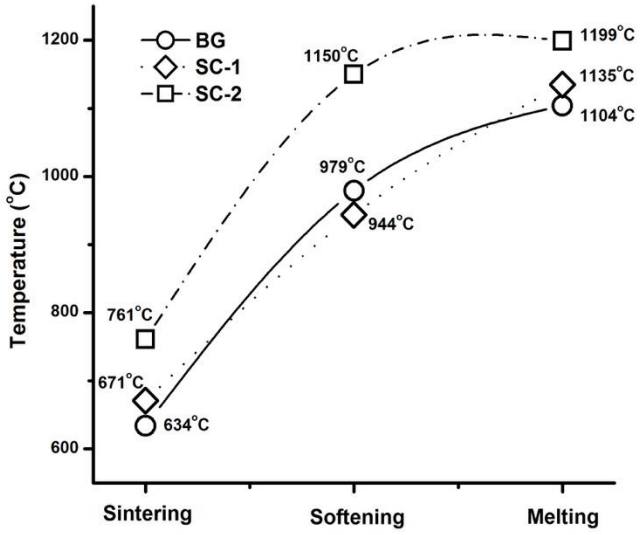

Figure 21. Hot stage microscopy testing of all three glasses with corresponding sintering, softening, and melting temperature for each glass.

1.7. Magic Angle Spinning Nuclear Magnetic Resonance (MAS-NMR)

Magic angle spinning-nuclear magnetic resonance (MAS-NMR) spectra of *BG*, *SC-1*, and *SC-2* is represented in Figure 22. Slight chemical peak shifts of -88.2 ppm to -87.1 ppm and -87.3 ppm can be observed for a.) *BG*, b.) *SC-1*, and c.) *SC-2*, respectively as shown in Figure 22. Peak broadening is also present where *BG* shows greater distribution of Q species with *SC-1* the most towards to Q^3 region as shown in Figure 22. Also, Q^0, Q^1, Q^2, Q^3, and Q^4 structures corresponds with in the chemical shift ranges from -60 to -80 ppm, -65 to -85 ppm, -75 to -95 ppm, -90 to -100 ppm, and -105 to 120 ppm, respectively [135]. This shift in the positive direction suggests that as Ti^{4+}-content replaces either Ca^{2+} or Na^{+}, it acts as intermediates and can bond to either Si^{4+} or O^{2-} within the network. Furthermore, peak shifts in the positive direction indicates the presence of lower order of SiO_4 tetrahedral coordination when Ti^{4+} is substituted for network modifiers.

MAS-NMR was conducted with the purpose of providing an in-depth evaluation of the glass network, specifically Si-coordination environment. For this study, ^{29}Si MAS-NMR was employed to determine any presence of chemical shifts characteristic corresponding to silicon atoms in tetrahedral coordination. Additionally, for further analysis on NMR spectra, each spectrum was deconvoluted where peak positions of the followings were used: Q^0 (-70 ppm), Q^1 (-80ppm), Q^2 (-85 ppm), Q^3 (-90 ppm), and Q^4 (-110 ppm). An average of reported peak positions for bioactive glass with metals were taken during the analysis in order to represent the glasses produced for this study [136-140].

Figure 23, 24, and 25 corresponds to deconvolution of NMR spectra on *BG*, *SC-1*, and *SC-2*, respectively. Deconvolution was performed in order to have better understanding of relative fractions of Q-species within the glass network. It is evident that *BG* mostly showed presence of Q^3 (68%) and Q^4 (17%) with 16% of Q^2 species present. However, both *SC-1* and *SC-2* showed greater distribution of Q-species where majority of the glass showed presence of Q^2 and Q^3 (where Q^3 was 48% and 60%, respectively) as shown in Figure 26. It is also evident that Q^1 species were absent in *BG* where 27% and 14% were present for *SC-1* and *SC-2*, respectively.

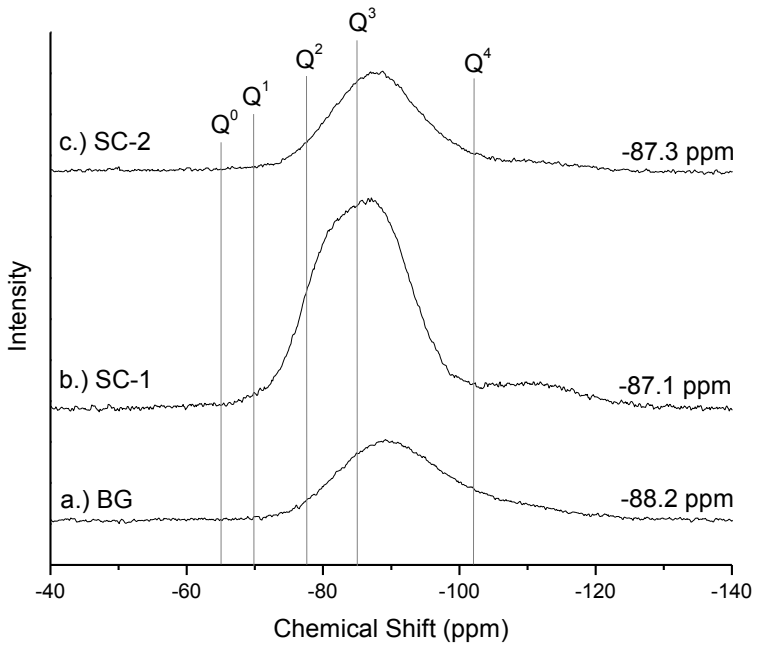

Figure 22. MAS-NMR spectra of all three glasses.

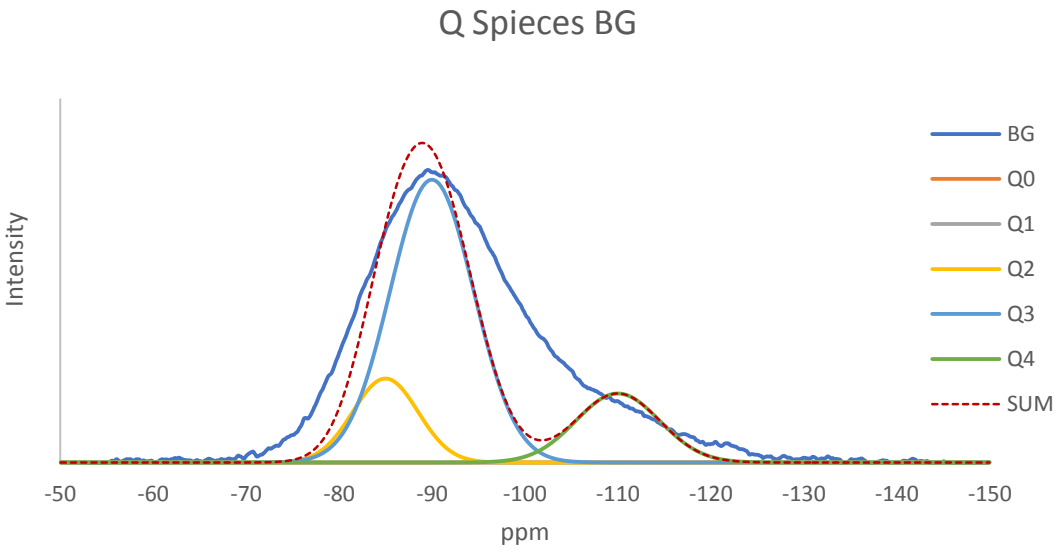

Figure 23. MAS-NMR spectra of *BG*.

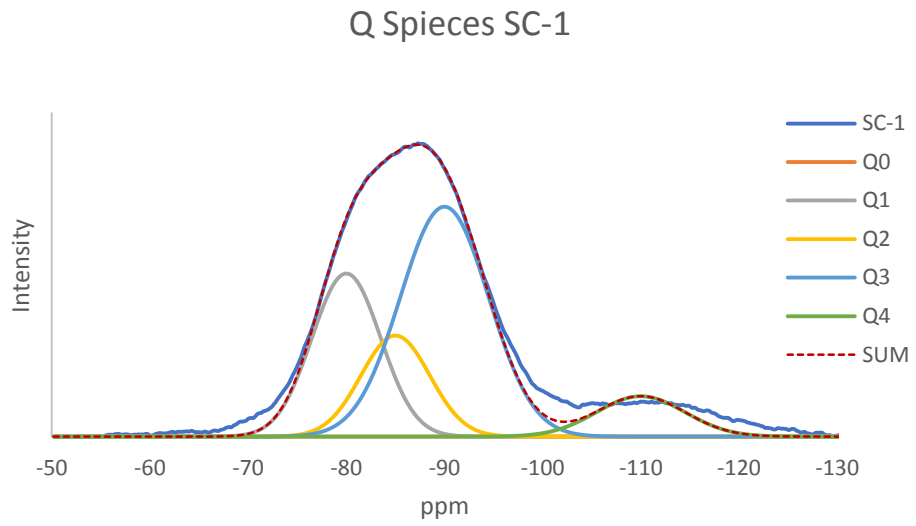

Figure 24. MAS-NMR spectra of *SC-1*.

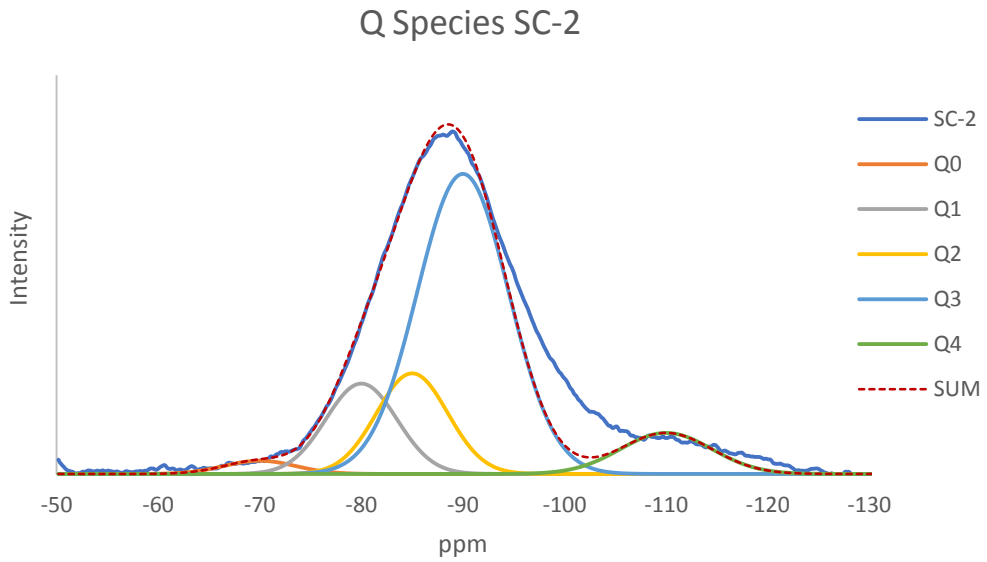

Figure 25. MAS-NMR spectra of *SC-2*.

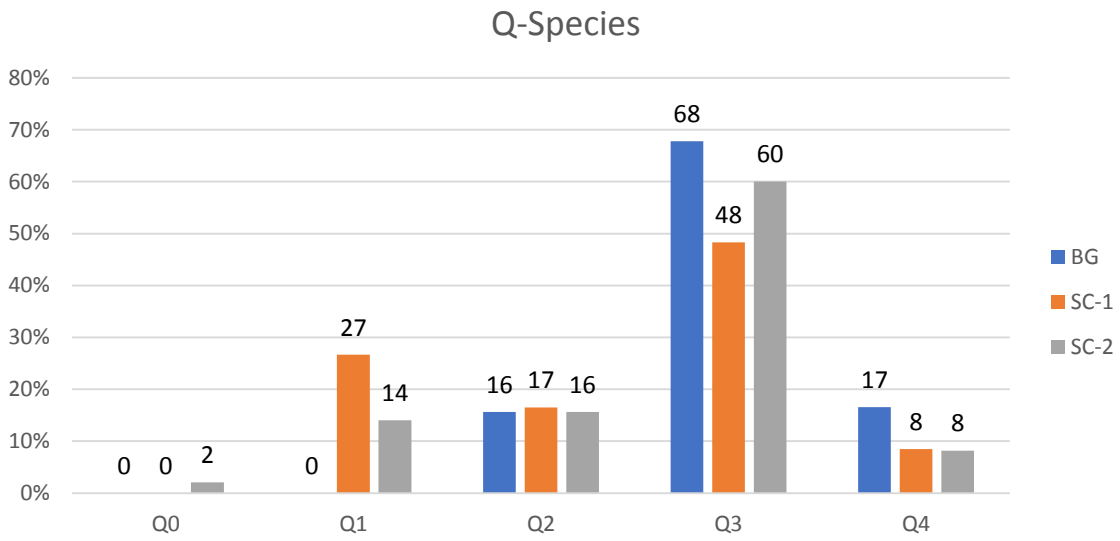

Figure 26. Q-Species percentage for all three glasses.

It is evident from Figure 26 that a decrease in Q^3 and Q^4 species can be observed when Ti is introduced into the glass network. Increase in Q^1 and Q^2 species of *SC-1* and *SC-2* also supports the effect of Ti forming TiO_4 and TiO_6 structures that can essentially have an influence on NMR spectra that detects Si-O bonds. Thus, broadening of spectra can be observed in Figure 22. Understanding the distribution of Q-species is important because the formation of non-bridging oxygens will have effect on glass solubility, which plays an important role of dissolution of the particle surface that initiates the bioactive sequence as mentioned in literature review.

2. Ti^{4+} Effect on Glass Solubility & *in vitro* Bioactivity

2.1. Scanning Electron Microscopy/Energy Dispersive Spectroscopy (SEM/EDS)

One of the key features of silicate bioactive glass is its low SiO_2 content for it to be soluble in biological environment [141]. Through the dissolution of network modifiers such as Na^+ and Ca^{2+} ions, SiO_2-rich layer initiates attraction of Ca and P ions leading an amorphous calcium phosphate deposition to form, which later crystallizes into hydroxyl-carbonate apatite (HCA) layer. Three bioactive glasses with different composition were incubated under SBF to determine the effect of TiO_2 on surface reactivity. Thus, after characterization of materials, simulated body fluid (SBF) was used to determine surface reactivity of bioactive glass with respect to (i) composition, and (ii) incubation periods of time, which was 1, 10, 100, and 1,000 hours.

SEM images of incubated samples and EDX (Figure 27, 28, and 29) represents semi-quantitative chemical analysis of all three glasses incubated at 1,000 hours. Figure 27 shows surface images of *BG* when incubated in SBF for 1 to 1,000 hours. Presence of calcium phosphate (CaP) deposition can be observed even at 1 hour. By 100 hours, dehydration cracks are present on the surface and precipitation all over the surface can be observed. At 1,000 hours, the surface is fully deposited with CaP. Corresponding EDX detected the presence of Ca at ~39 wt% and P at ~13 wt% while Si was detected at ~2.62 wt% as shown in Figure 27.

SEM image of *SC-1* and *SC-2* is represented in Figure 28 and Figure 29, respectively. At SBF incubation of 1 and 10 hours, *SC-1* shows partial deposition of CaP but at 100 and 1,000 hours, traces of CaP deposition cannot be observed as shown in Figure 28. Corresponding EDX of 1,000 hours incubated *SC-1* show slight increase in Ca and P content but high presence of Si at ~ 22 wt% was present. Figure 29 shows surface images of *SC-2* where CaP deposition was not present on any samples incubated over 1, 10, 100, and 1,000 hours. Corresponding EDX results indicate low presence of Ca and P compare to *BG* at ~18 and ~5 wt%, respectively.

It is evident that *BG,* a control, exhibited excellent calcium phosphate deposition on the surface over incubation time. SEM image of *BG* incubated at 1 and 10 hours

showed partial deposition of calcium phosphate on the surface of the glass in a shape similar to earlier findings on TiO_2 containing bioceramics [33]. After 100 hours, calcium phosphate deposition took a shape of microspheres spread across the surface of the material as well as stacked upon each other. At 1,000 hours, it is clearly visible that the calcium phosphate deposition formed a layer on top of the surface as shown in Fig. 27. Also, cracks on the surface of *BG* can be attributed to dehydration during preparation for analysis. High concentrations of calcium phosphate on the surface were evident as expected. However, *SC-1* and *SC-2* showed dramatically different results. Both glasses did not show any visible indication of the deposition layer present on the surface. Previous studies done by Cormier *et al.* have shown through X-ray absorption spectroscopy that TiO_2 acts as nucleating agent within glass network [142] and the dissolution rate of a glass was expected to decrease when a crystalline phase was present. Furthermore, Clupper and Hench stated the crystal phase of $Na_2Ca_2Si_3O_9$ within Bioglass® has slightly decreased the formation kinetics of an apatite layer on the surface of the sample [143-146].

Not only in the silicate glass system but a study on the increase of TiO_2 content beyond 0.5 mol% within borate glass system reported in possible formation of either TiO_5 or TiO_4 that strengthens the glass network, which can hinder the ability of the glass to create calcium phosphate deposition layer similar to bioactive glass without any TiO_2 in the system [83]. In other words, SEM images of *SC-1* and *SC-2* without any visible deposition can be supported by the formation of Q^1 and Q^2 species along with peak broadening that was evident from MAS-NMR spectra, which could result from formation of TiO_4 and TiO_6.

Although, the formation of calcium phosphate deposition is not entirely visible in Fig. 28 and 29, numerous studies have reported that Ti containing materials result in calcium phosphate deposition on the surface when incubated in SBF [33,147].

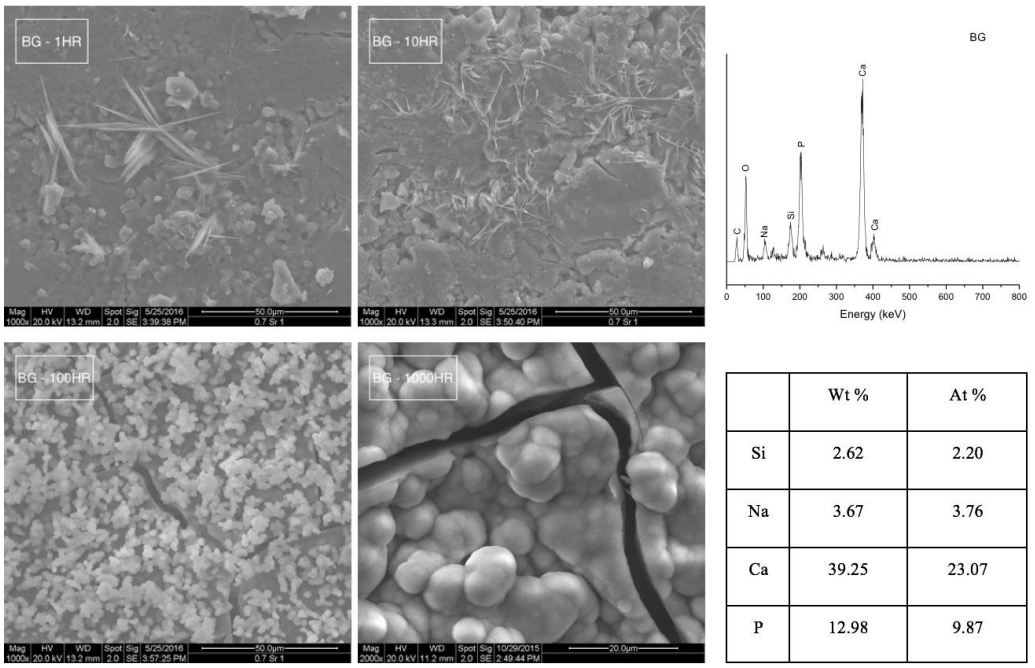

	Wt %	At %
Si	2.62	2.20
Na	3.67	3.76
Ca	39.25	23.07
P	12.98	9.87

Figure 27. SEM images of *BG* after 1, 10, 100, and 1,000 hours in SBF with EDS result after 1,000 hours of incubation.

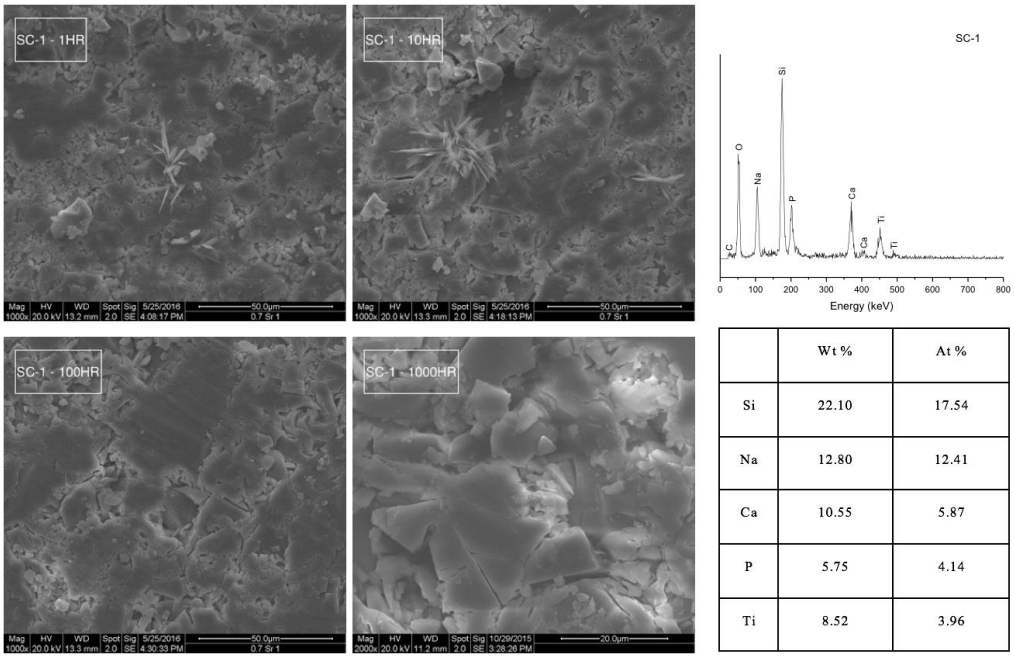

	Wt %	At %
Si	22.10	17.54
Na	12.80	12.41
Ca	10.55	5.87
P	5.75	4.14
Ti	8.52	3.96

Figure 28. SEM images of *SC-1* after 1, 10, 100, and 1,000 hours in SBF with EDS result after 1,000 hours of incubation.

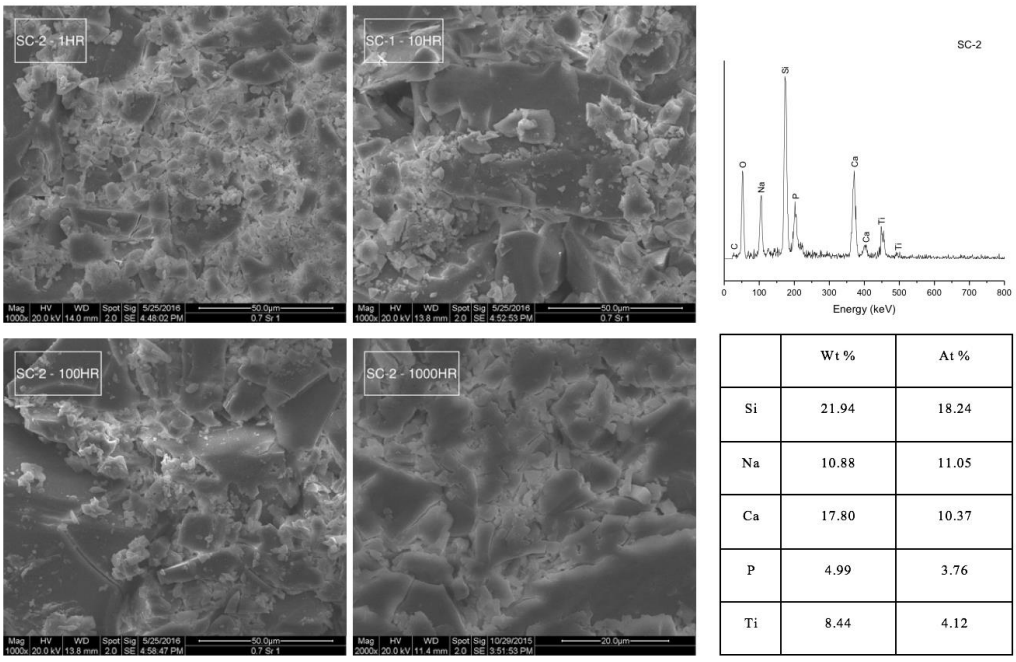

	Wt %	At %
Si	21.94	18.24
Na	10.88	11.05
Ca	17.80	10.37
P	4.99	3.76
Ti	8.44	4.12

Figure 29. SEM images of *SC-2* after 1, 10, 100, 1,000 hours in SBF with EDS result after 1,000 hours of incubation.

2.2. Inductively Coupled Plasma-Optical Emission Spectroscopy (ICP-OES)

One of the concerns for common silicate bioactive glass such as 45S5 Bioglass® is poor mechanical durability under SBF due to high dissolution rate. Although Lai *et al.* have reported the release of Si^{4+} in the form of silicic acid, $Si(OH)_4$, was excreted through the urine harmlessly in rabbits [148], the biological effects on the changes of pH due to release of various ions has yet to be fully understood [141]. Furthermore, studies by Tousi *et al.* have shown that the release of both Si^{4+} and Ca^{2+} into the biological environment enhanced bio-mineralization of osteoblast cells through enhanced osteocalcin expression [87]. Thus, ion release profile and pH measurements were performed in order to understand more on the effect of TiO_2 in dissolution rate as well as its relationship to the pH of SBF extracts and to further investigate the absence of CaP deposition on Ti containing glasses.

Ion release profiles of *BG*, *SC-1*, and *SC-2* were determined with respect to incubation time where Figure 30 represents the ion release profile for *BG* where increase in Na^+ level from 724 to 1154 mg/L over 1 to 100 hours can be observed. However, Na^+ level decreased from 1154 to 1088 mg/L at 1,000 hours of incubation time. Si^{4+} on the other hand, showed consistent increase from 1 to 12 mg/L over 1 to 1,000 hours of incubation time. Ca^{2+} and P^{5+} show gradual decrease with a slight increase in Ca^{2+} level at 100 hours from 26 to 3 mg/L and 9 to 0.4 mg/L, respectively. Figure 31 represents the ion release profile for *SC-1* where slight increase of Na^+ level can be observed from 739 to 983 mg/L compare to *BG*. Si^{4+} level decreased from 1.3 to 0.9 mg/L at 10 hours and increased up to 4 mg/L at 1,000 hours. Ca^{2+} and P^{5+} level show slight decrease from 15 to 18 mg/L and 7 to 5 mg/L, respectively. However, Ti^{4+} level remained 0 through the incubated periods of time. Figure 32 represents the ion release profile for *SC-2* where Na^+ level show gradual increase from 708 to 1023 mg/L and Si^{4+} level increased from 1.2 to 1.3 at 10 hours, decreased down to 0.1 mg/L at 100 hours but increased up to 3.6 mg/L at 1,000 hours. Ca^{2+} level stayed almost same with the difference of 2 mg/L over the periods of incubated time where it increased at 1,000 hours similar to P^{5+} level. Ion release profile of *SC-2* also showed Ti^{4+} level at 0 mg/L throughout the incubation of 1, 10, 100, and 1,000 hours.

It is evident from Fig. 30 that overall release of ions in *BG* was much greater than *SC-1* or *SC-2*, which was expected because Ti strengthens the glass network, which lowers dissolution rate. Also, constant increase in Si from Fig. 30 represents dissolution of Si possibly forming SiO_2-rich layer on the surface, which then attracts ions such as Ca and P to form calcium phosphate deposition that can be explained by overall decrease of both Ca and P with the increase in incubation time. *SC-1* also showed overall decrease in Ca and P with increase in Si release over incubation time as shown in Figure 31. However, the rate of dissolution of *SC-1* was significantly lower than *BG* indicating titanium does play a role in decreasing dissolution rate of bioactive glass. Although the calcium phosphate deposition on the surface of *SC-1* was not visibly clear with SEM images, ion release profile showed the evidence of dissolution and the overall decrease in Ca and P, which supported very low amounts of calcium deposition on the surface layer of the glass. On the other hand, *SC-2* exhibited slight decrease in Ca content up until 1,000 hours where a slight increase can be observed as shown in Figure 32. Study done by Santos *et al.* have reported decrease in calcium deposition layer on the surface of bioactive glass over incubation time due to surface degradation under aqueous media [149], which can explain a sudden increase in both Ca and Si release rate of *SC-2* after incubation time of 1,000 hours in Figure 32. Unlike other ions, Ti^{4+} was not released from both *SC-1* and *SC-2* as shown in Figure 31 and 32, respectively. It was reasonable to see the absence of Ti^{4+} released into the SBF because it's been suggested that due to small ionic radius and a large electric charge, Ti^{4+} ions can bond with Si forming Si-O-Ti bonds. Also, Ti^{4+} plays a role in restricting both P and Ca ion release, which explains lower release rate of modifying ions of *SC-1* and *SC-2* compare to a control, *BG* [150].

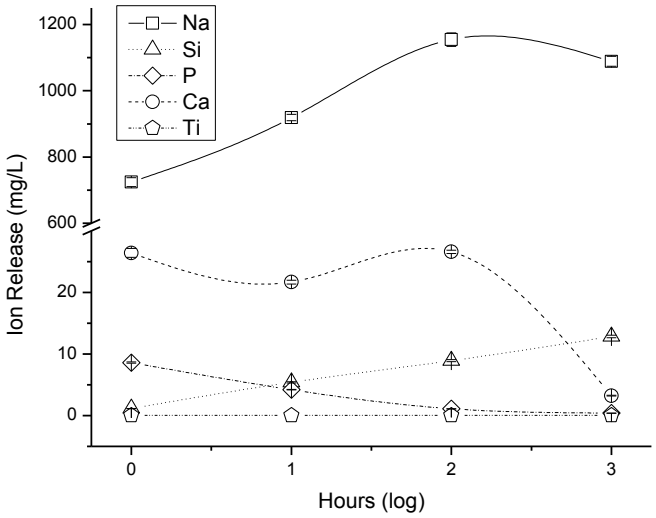

Figure 30. Ion release profile of *BG* investigating Na, Si, P, Ca, and Ti release rate after incubation time of 1, 10, 100, and 1,000 hours in SBF.

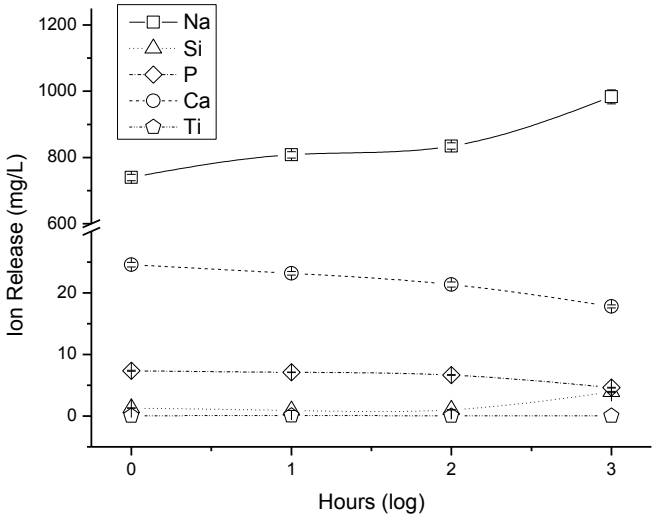

Figure 31. Ion release profile of *SC-1* investigating Na, Si, P, Ca, and Ti release rate after incubation time of 1, 10, 100, and 1,000 hours in SBF.

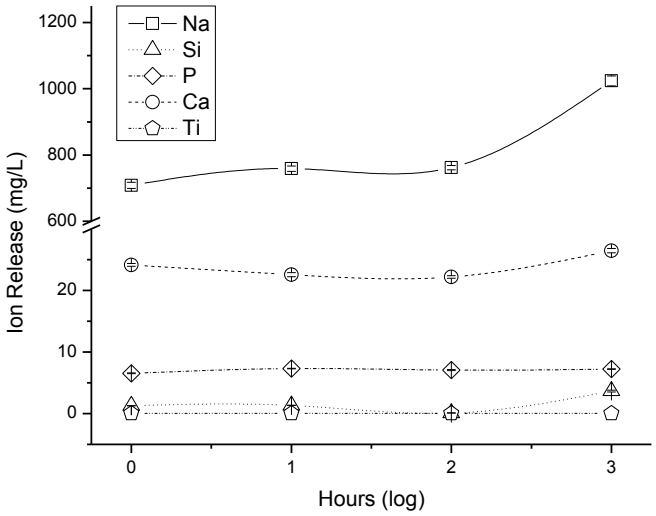

Figure 32. Ion release profile of *SC-2* investigating Na, Si, P, Ca, and Ti release rate after incubation time of 1, 10, 100, and 1,000 hours in SBF.

2.3. pH Analysis

As mentioned above, such release of various ions from the material into the biological fluid can alter the pH of the biological environment, or the simulated body fluid in this case. The pH of each SBF extract was measured with respect to glass composition and incubation time, and Figure 33 represents the change in pH of SBF extracts after 1, 10, 100, 1,000 hours. It is evident from Figure 33 that *BG* showed the highest increase in pH over the incubation period where the pH increased from 7.9 to 9.2, which corresponds with the ion release results. *SC-1* and *SC-2* showed no significant difference in pH from 1 to 10 hours where decrease in ph of SBF extracts of both *SC-1* and *SC-2* were less than 0.1. After 100 hours, both extracts of *SC-1* and *SC-2* showed an increase up to 8.4 and 7.9, respectively.

Increase in pH can be explained through the release of network modifiers such as Na^{+} or Ca^{2+} ions into the SBF over time where slight drop in pH for *SC-1* and *SC-2* at 1 hour of incubation indicated the release of Si^{4+} into the SBF. The range of pH corresponded with the range reported for Bioglass® through a study done by Chen *et al.* where the pH of biological fluid extract ranged from pH of 9 to 11 [34]. The initial release of Si^{4+} into the SBF can cause Si-OH group to form on the surface, which then attracts Ca and P to form an amorphous calcium phosphate deposition layer. It is likely that the crystalline phase reported by XRD pattern for *SC-1* and *SC-2* due to substitution of TiO_2 reduced the dissolution rate and thus causing delayed change in pH of the SBF extracts. For instance, higher crystallinity observed for *SC-2* may have caused much lower change in pH compared to *SC-1* with lower crystallinity phase in the glass. However, not only the crystallinity, but Ti^{4+} plays a role in strengthening the glass network *via* bonding with both network former and modifiers as supported by increase in T_g present in DTA result as well as peak shifts in positive direction shown by MAS-NMR results. In other words, it is evidently supported by various characterization techniques that Ti^{4+} plays an intermediate role within bioactive glass network.

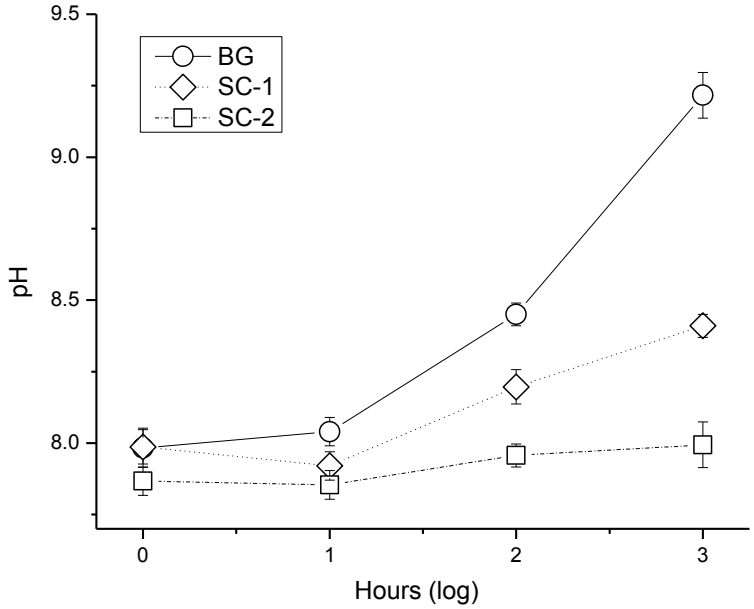

Figure 33. pH of incubated SBF extracts after 1, 10, 100, and 1,000 hours.

2.4. Hardness Testing

Silicate bioactive glass networks exhibit promising properties for the use of bone tissue engineering application. The ability to form an amorphous calcium phosphate deposition, which later then crystallizes into a HCA layer for osteoblast colonization is a significant advantage regarding biomedical applications. However, aside from high dissolution rate for silicate bioactive glasses, another major concern is the change in mechanical properties when these materials are immersed within a biological environment. This behavior is called chemo-mechanical behavior, which is indicated by any changes in mechanical properties due to reactions with a biological environment [151]. When bioactive glasses are fabricated into scaffolds, their hardness and compressive strength is very poor. As a result, a better understanding of the relationship between the mechanical properties and dissolution characteristics needs to be further researched. In order to overcome such current limitations of regular bioactive glass series, hardness testing was conducted on TiO_2 containing glasses, *SC-1* and *SC-2* and compared with the result of the control glass, *BG*.

The hardness testing result of all glasses incubated in SBF for 1, 10, 100, and 1,000 hours where the hardness strength of the glass samples was plotted as a function of incubation time (Figure 34). It is evident that the hardness of *BG* was significantly lower compared to both *SC-1* and *SC-2*. Moreover, decrease in hardness of *BG* from 1.01 to 0.75 GPa after 1,000 hours can be observed. *SC-1* and *SC-2* also exhibited similar trend where the hardness of the glasses has decreased over the incubation time. The hardness of *SC-1* slightly increased from 2.15 to 2.23 GPa from 1 to 10 hours of incubation but it significantly dropped to 1.90 and 1.06 GPa after 100 and 1,000 hours, respectively. On the other hand, *SC-2* showed constant decrease in hardness of the sample over incubation time from 2.30 to 1.67, 1.16, and 1.09 GPa for 1, 10, 100, and 1,000 hours, respectively. It is also clear that *SC-1* and *SC-2* showed higher hardness when compared to the control, *BG*.

It is clear from Figure 34 that both *SC-1* and *SC-2*, which contain TiO_2, showed a significant difference in hardness compared to *BG* even after 1,000 hours of incubation under SBF. The highest value obtained for *BG* was 1.01 GPa where the lowest value obtained for *SC-1* and *SC-2* were 1.06 and 1.79 GPa, respectively. All three glasses

showed a decrease in hardness over series of incubation times, which was expected due to dissolution of the glass and chemical changes such as formation of SiO_2-rich and calcium phosphate deposition layer. The slight increase in hardness strength of *SC-1* after 10 hours can possibly be explained by fast formation of SiO_2-rich layer on the surface of the glass. *SC-2* does not show such behavior because there are more Na_2O in *SC-1* compare to *SC-2*. A previous study showed that the increase in Na_2O enhances bioactivity because Na-Ca-Si-O phases are introduced into the system, which are biodegradable [34]. Thus, due to enhanced bioactivity of *SC-1* compared to *SC-2,* chemical change on the surface may have caused a slight change in mechanical properties. It has been shown that the substitution of TiO_2 within bioactive glass has drastically increased the initial hardness strength of the glass as expected. This may not only be a result of increase in glass network stability as shown by thermal analysis but also a result of higher distribution of Q-species that was observed *via* MAS-NMR for both *SC-1* and *SC-2*. Furthermore, it is reasonable to state no significant difference in hardness based on the amount of crystallinity present in the glass as similar mechanical characteristic can be observed for both *SC-1* and *SC-2*.

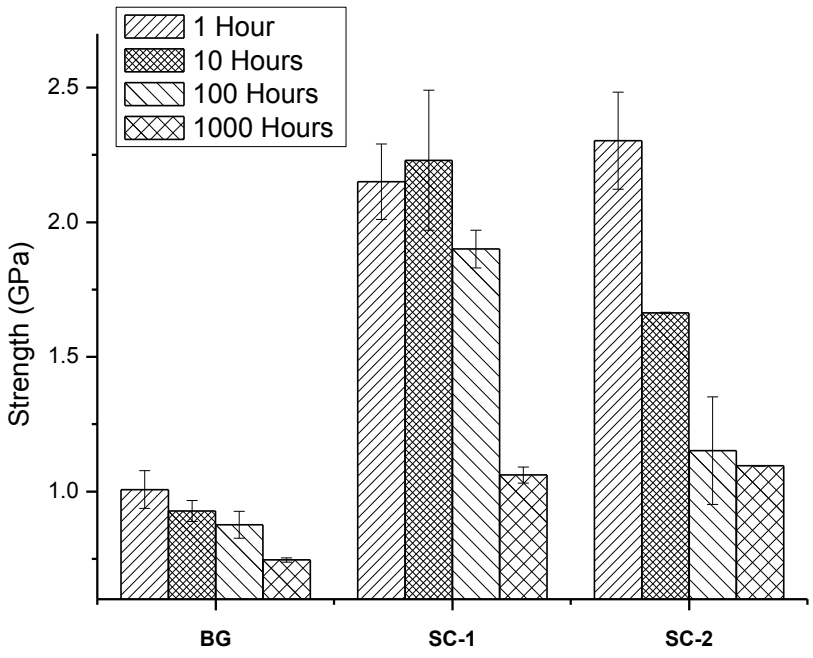

Figure 34. Hardness testing of all three glasses after incubation under SBF for 1, 10, 100, and 1,000 hours.

3. Scaffold Synthesis & Characterization

3.1. X-ray Diffraction (XRD)

Scaffolds were fabricated using the foam replication procedure where scaffolds were heat treated at various temperatures below the sintering temperature measured by HSM. *SC-1* was selected for scaffold synthesis based on absence of crystallization temperature determined by thermal analysis and partial crystallinity at initial glass powder identified by X-ray diffraction. *BG* did not form a stable scaffold to pursue further characterization. Different temperatures were used to heat treat the scaffolds to determine the transition of scaffolds into the vitreous state. Temperatures of 600, 610, 620, and 635°C were selected where Figure 35 represents X-ray diffraction pattern of *SC-1* derived scaffolds heat treated at the specified temperature points.

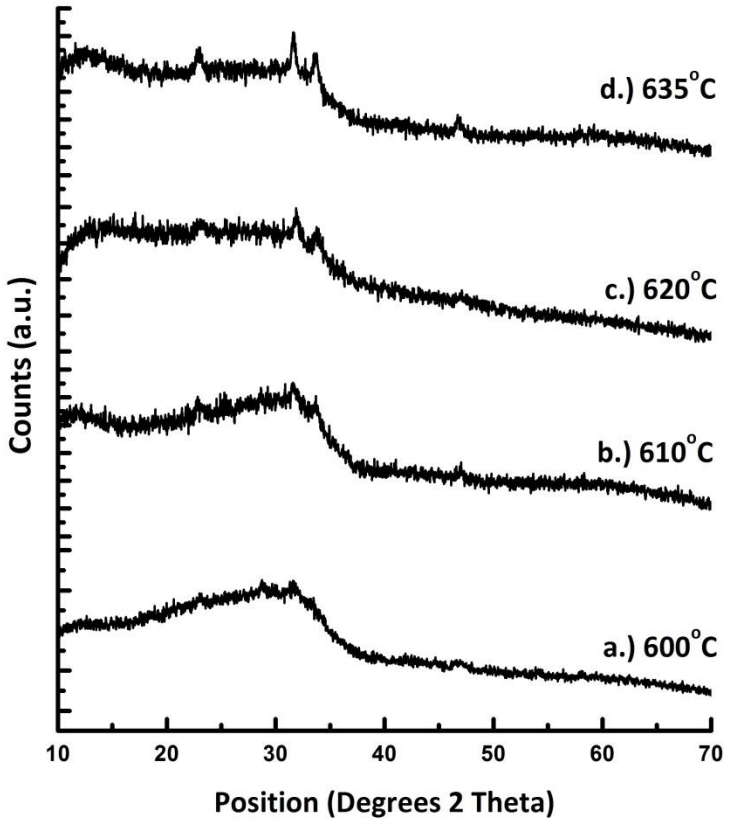

Figure 35. X-ray diffraction pattern of *SC-1* derived scaffolds fabricated at different heat treatment temperatures.

3.2. Optical Imaging

Optical stereomicroscopes of the scaffolds synthesized at each temperature are presented in Figure 36. It is evident that transitions of powdered material into a vitreous scaffold are present within the sintering temperature range of 600 to 635°C. Furthermore, visible evidence of light-reflecting structure correlates with the reported X-ray diffraction pattern as shown in Figure 35. Although low crystallinity can be observed with both X-ray diffraction pattern and optical stereomicroscopy, such results show promising glass composition type and fabrication parameters to fabricate amorphous bioactive glass derived scaffolds.

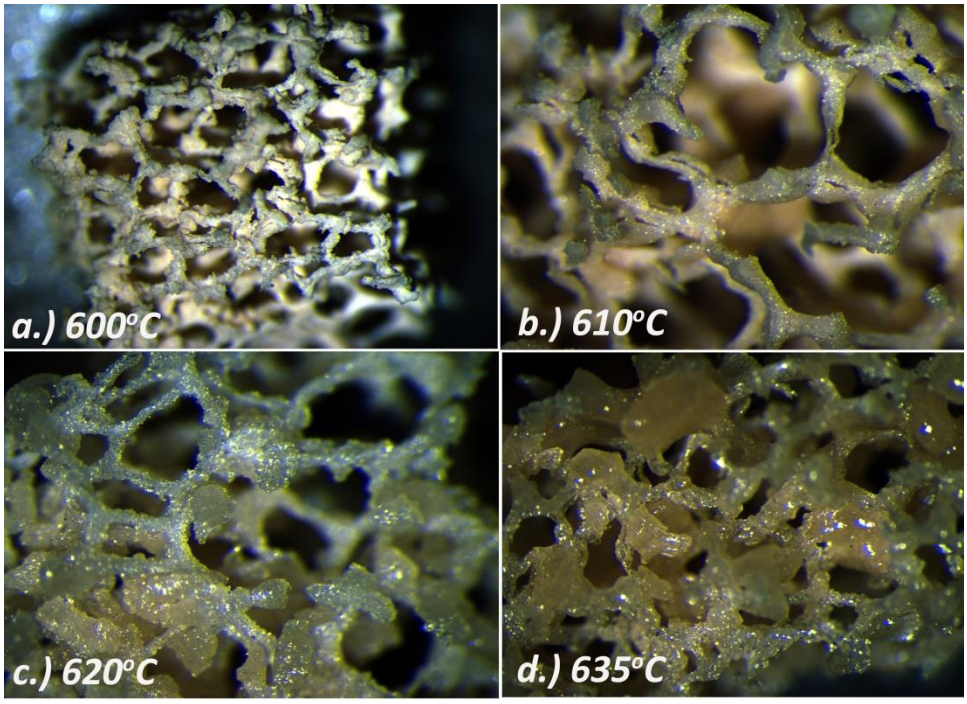

Figure 36. Optical image of *SC-1* derived scaffold fabricated at different heat treatment temperatures.

SUMMARY AND CONCLUSIONS

The purpose of this study was to: (i) investigate the effect of TiO_2 substitution for network modifiers within SiO_2-CaO-Na_2O-P_2O_5 bioactive glass system, (ii) evaluate and select appropriate glass composition to fabricate mechanically stable amorphous scaffold. The addition of TiO_2 influenced initial crystallinity of the glass in powder form and thermal analysis showed absence of crystallization (vitrification) temperatures. Results showed modified glass structure of increased fraction of non-bridging oxygen (NBO^-) in the glass but the ion release of Si showed drastic decrease, which explains no visual evidence of calcium phosphate precipitation on the surface after SBF incubation. Although BG showed higher amount of CaP deposition layer on the surface, substitution of TiO_2 led to stabilized ion release where pH of media fluids showed lower magnitude of change over incubation time. Furthermore, the inclusion of TiO_2 significantly improved the mechanical stability where *SC-1* and *SC-2* showed greater hardness strength even after 1,000 hours of incubation time. Based on the results, *SC-1*, where TiO_2 was substituted with CaO, showed the ability to fabricate amorphous scaffold at low temperature of (~635°C). It was evident that increase in mechanical stability of initial glass due to inclusion of TiO_2 was represented well after fabrication into scaffold because *BG* was not selected for further characterization study due to its poor mechanical stability. Therefore, studies have shown the substitution of TiO_2 for network modifier instead of network former can grant the ability to synthesize mechanically stable scaffolds while retaining its amorphous structure for better bioactivity compared to currently known bioactive glass derived scaffolds.

FUTURE WORK

The main objective of this study was to fabricate bioactive glass derived scaffold with modified glass composition in order to compensate common drawbacks that are currently challenging to overcome. After characterization and evaluation of modified glass compositions, *SC-1* was selected and produced into scaffolds where amorphous scaffolds were achieved below the sintering temperature when heat treated. Although X-ray diffraction and optical stereomicroscopy were performed on the scaffolds, more initial characterizations are required in the future. For instance, quantitative measurement of porosity to ensure that fabricated scaffold meets the required characteristics of an ideal scaffold used in bone tissue engineering. Additionally, mechanical characterization when incubated in SBF to investigate the potential ability to induce cell attachment and proliferation, specifically osteoblast cells. Such fabricated scaffolds are expected to show higher mechanical stability due to significant differences in hardness of the initial glass composition and better cell adhesion with higher cell viability due to more controlled dissolution rate of ions when introduced in simulated body fluid.

REFERENCES

1. A. K. Varshneya, "Chapter 3 - Glass Formation Principles"; pp. 27-59 in *Fundamentals of Inorganic Glasses.* Academic Press, San Diego, 1994.

2. J. E. Shelby, *Introduction to Glass Science and Technology*. Royal Society of Chemistry, 2005.

3. A. K. Varshneya, "Chapter 4 - Glass Microstructure: Phase Separation and Liquid Immiscibility"; pp. 61-86 in *Fundamentals of Inorganic Glasses.* Academic Press, San Diego, 1994.

4. W. H. Zachariasen, "The Atomic Arrangement in Glass," *J. Am. Chem. Soc.,* **54** [10] 3841-51 (1932).

5. R. G. Iacocca and M. Allgeier, "Corrosive Attack of Glass by a Pharmaceutical Compound," *J. Mater. Sci.,* **42** [3] 801-11 (2007).

6. D. E. Clark, C. G. Pantano Jr, and L. L. Hench, "Corrosion of Glass," (1979).

7. G. A. Cox and B. A. Ford, "The Long-Term Corrosion of Glass by Ground-Water," *J. Mater. Sci.,* **28** [20] 5637-47 (1993).

8. A. El-Ghannam, E. Hamazawy, and A. Yehia, "Effect of Thermal Treatment on Bioactive Glass Microstructure, Corrosion Behavior, Z Potential, and Protein Adsorption," *J. Biomed. Mater. Res.,* **55** [3] 387-95 (2001).

9. P. Valerio, M. M. Pereira, A. M. Goes, and M. F. Leite, "The Effect of Ionic Products from Bioactive Glass Dissolution on Osteoblast Proliferation and Collagen Production," *Biomaterials,* **25** [15] 2941-8 (2004).

10. L. L. Hench, "The Story of Bioglass®," *J. Mater. Sci. Mater. Med.,* **17** [11] 967-78 (2006).

11. L. L. Hench, R. J. Splinter, W. C. Allen, and T. K. Greenlee, "Bonding Mechanisms at the Interface of Ceramic Prosthetic Materials," *J. Biomed. Mater. Res.,* **5** [6] 117-41 (1971).

12. S. Piscanec, L. C. Ciacchi, E. Vesselli, G. Comelli, O. Sbaizero, S. Meriani, and A. De Vita, "Bioactivity of Tin-Coated Titanium Implants," *Acta Materialia,* **52** 1237-45 (2004).

13. A. Laptev, M. Bram, H. P. Buchkremer, and D. Stöver, "Study of Production Route for Titanium Parts Combining Very High Porosity and Complex Shape," *Powder Metall.,* **47** [1] 85-92 (2004).

14. B. Feng, J. Weng, B. C. Yang, S. X. Qu, and X. D. Zhang, "Characterization of Titanium Surfaces with Calcium and Phosphate and Osteoblast Adhesion," *Biomaterials,* **25** [17] 3421-8 (2004).

15. W. Chrzanowski, E. A. A. Neel, D. A. Armitage, and J. C. Knowles, "Effect of Surface Treatment on the Bioactivity of Nickel–Titanium," *Acta Biomaterialia,* **4** [6] 1969-84 (2008).

16. M. Yoshinari, Y. Oda, T. Kato, and K. Okuda, "Influence of Surface Modifications to Titanium on Antibacterial Activity in Vitro," *Biomaterials,* **22** [14] 2043-8 (2001).

17. B. Feng, J. Chen, and X. Zhang, "Interaction of Calcium and Phosphate in Apatite Coating on Titanium with Serum Albumin," *Biomaterials,* **23** [12] 2499-507 (2002).

18. L. L. Hench and J. M. Polak, "Third-Generation Biomedical Materials," *Science,* **295** [5557] 1014 (2002).

19. V. Guarino, F. Causa, and L. Ambrosio, "Bioactive Scaffolds for Bone and Ligament Tissue," *Expert Rev. Med. Devices,* **4** [3] 405-18 (2007).

20. D. W. Hutmacher, J. T. Schantz, C. X. F. Lam, K. C. Tan, and T. C. Lim, "State of the Art and Future Directions of Scaffold-Based Bone Engineering from a Biomaterials Perspective," *J. Tissue Eng. Regen. Med.,* **1** [4] 245-60 (2007).

21. J. R. Jones, "New Trends in Bioactive Scaffolds: The Importance of Nanostructure," *J. Eur. Ceram. Soc.,* **29** [7] 1275-81 (2009).

22. Q.-Z. Chen, K. Rezwan, V. Françon, D. Armitage, S. N. Nazhat, F. H. Jones, and A. R. Boccaccini, "Surface Functionalization of Bioglass®-Derived Porous Scaffolds," *Acta Biomaterialia,* **3** [4] 551-62 (2007).

23. X. Chen, Y. Meng, Y. Li, and N. Zhao, "Investigation on Bio-Mineralization of Melt and Sol-Gel Derived Bioactive Glasses," *Appl. Surf. Sci.,* **255** [2] 562-4 (2008).

24. G. Radha and K. Ashok, "Bioactive Materials for Biomedical Applications Using Sol–Gel Technology," *Biomed. Mater.,* **3** [3] 034005 (2008).

25. L. L. Hench, "Bioceramics: From Concept to Clinic," *J. Am. Ceram. Soc.,* **74** [7] 1487-510 (1991).

26. S. Salman, S. Salama, and H. Abo-Mosallam, "The Crystallization Behaviour and Bioactivity of Wollastonite Glass-Ceramic Based on Na 2 O–K 2 O–Cao–Sio 2–F Glass System," *Journal of Asian Ceramic Societies,* **3** [3] 255-61 (2015).

27. J. J. Blaker, S. N. Nazhat, and A. R. Boccaccini, "Development and Characterisation of Silver-Doped Bioactive Glass-Coated Sutures for Tissue Engineering and Wound Healing Applications," *Biomaterials,* **25** [7–8] 1319-29 (2004).

28. J. R. Jones, "Bioactive Ceramics and Glasses," *Tissue engineering using ceramics and polymers,* **1** 52-71 (2007).

29. T. J. Brunner, R. N. Grass, and W. J. Stark, "Glass and Bioglass Nanopowders by Flame Synthesis," *Chem. Commun.*, [13] 1384-6 (2006).

30. L. Hench and J. Jones, *Biomater., Artif. Organs and Tissue Eng.,* Elsevier, 2005.

31. A. R. Boccaccini, Q. Chen, L. Lefebvre, L. Gremillard, and J. Chevalier, "Sintering, Crystallisation and Biodegradation Behaviour of Bioglass®-Derived Glass–Ceramics," *Faraday Discuss.,* **136** 27-44 (2007).

32. I. D. Thompson and L. L. Hench, "Mechanical Properties of Bioactive Glasses, Glass-Ceramics and Composites," *Proc. Inst. Mech. Eng., Part H,* **212** [2] 127-36 (1998).

33. Y. Li, A. Coughlan, and A. W. Wren, "Investigating the Surface Reactivity of Sio2–Tio2–Cao–Na2o/Sro Bioceramics as a Function of Structure and Incubation Time in Simulated Body Fluid," *J. Mater. Sci. Mater. Med.,* **25** [8] 1853-64 (2014).

34. Y. Li, A. Coughlan, F. R. Laffir, D. Pradhan, N. P. Mellott, and A. W. Wren, "Investigating the Mechanical Durability of Bioactive Glasses as a Function of Structure, Solubility and Incubation Time," *J. Non-Cryst. Solids,* **380** 25-34 (2013).

35. L. G. Donaruma, "Definitions in Biomaterials, D. F. Williams, Ed., Elsevier, Amsterdam, 1987, 72 Pp," *J. Polym. Sci., Part C: Polym. Lett.,* **26** [9] 414- (1988).

36. H. Oonishi, L. L. Hench, J. Wilson, F. Sugihara, E. Tsuji, S. Kushitani, and H. Iwaki, "Comparative Bone Growth Behavior in Granules of Bioceramic Materials of Various Sizes," *J. Biomed. Mater. Res.,* **44** [1] 31-43 (1999).

37. L. C. Gerstenfeld, D. M. Cullinane, G. L. Barnes, D. T. Graves, and T. A. Einhorn, "Fracture Healing as a Post-Natal Developmental Process: Molecular,

Spatial, and Temporal Aspects of Its Regulation," *J. Cell. Biochem.*, **88** [5] 873-84 (2003).

38. T. A. Einhorn, "The Cell and Molecular Biology of Fracture Healing," *Clin. Orthop. Relat. Res.*, **355** S7-S21 (1998).

39. M. E. Bolander, "Regulation of Fracture Repair by Growth Factors," *Exp. Biol. Med.*, **200** [2] 165-70 (1992).

40. A. Schindeler, M. M. McDonald, P. Bokko, and D. G. Little, "Bone Remodeling During Fracture Repair: The Cellular Picture"; pp. 459-66 in Vol. 19. Elsevier,

41. G. L. Barnes, P. J. Kostenuik, L. C. Gerstenfeld, and T. A. Einhorn, "Growth Factor Regulation of Fracture Repair," *J. Bone Miner. Res.*, **14** [11] 1805-15 (1999).

42. I. H. Kalfas, "Principles of Bone Healing," *Neurosurg. Focus*, **10** [4] 1-4 (2001).

43. M. M. L. Deckers, R. L. Van Bezooijen, G. Van Der Horst, J. Hoogendam, C. van der Bent, S. E. Papapoulos, and C. W. G. M. Löwik, "Bone Morphogenetic Proteins Stimulate Angiogenesis through Osteoblast-Derived Vascular Endothelial Growth Factor A," *Endocrinology*, **143** [4] 1545-53 (2002).

44. D. I. Chen, M. Zhao, and G. R. Mundy, "Bone Morphogenetic Proteins," *Growth Factors*, **22** [4] 233-41 (2004).

45. T. Nakase and H. Yoshikawa, "Potential Roles of Bone Morphogenetic Proteins (Bmps) in Skeletal Repair and Regeneration," *J. Bone Miner. Metab.*, **24** [6] 425-33 (2006).

46. D. Baksh, L. Song, and R. S. Tuan, "Adult Mesenchymal Stem Cells: Characterization, Differentiation, and Application in Cell and Gene Therapy," *J. Cell. Mol. Med.*, **8** [3] 301-16 (2004).

47. C. Colnot, S. Huang, and J. Helms, "Analyzing the Cellular Contribution of Bone Marrow to Fracture Healing Using Bone Marrow Transplantation in Mice," *Biochem. Biophys. Res. Commun.*, **350** [3] 557-61 (2006).

48. H. Peng, A. Usas, A. Olshanski, A. M. Ho, B. Gearhart, G. M. Cooper, and J. Huard, "Vegf Improves, Whereas Sflt1 Inhibits, Bmp2-Induced Bone Formation and Bone Healing through Modulation of Angiogenesis," *J. Bone Miner. Res.*, **20** [11] 2017-27 (2005).

49. T. Tarkka, A. Sipola, T. Jämsä, Y. Soini, S. Ylä-Herttuala, J. Tuukkanen, and T. Hautala, "Adenoviral Vegf-a Gene Transfer Induces Angiogenesis and Promotes Bone Formation in Healing Osseous Tissues," *J. Gene Med.*, **5** [7] 560-6 (2003).

50. S. L. Teitelbaum, "Bone Resorption by Osteoclasts," *Science,* **289** [5484] 1504-8 (2000).

51. B. L. Riggs and L. J. Melton, 3rd, "The Worldwide Problem of Osteoporosis: Insights Afforded by Epidemiology," *Bone,* **17** [5] S505-S11 (1995).

52. A. Klibanski, L. Adams-Campbell, T. L. Bassford, S. N. Blair, S. D. Boden, K. Dickersin, D. R. Gifford, L. Glasse, S. R. Goldring, and K. Hruska, "Osteoporosis Prevention, Diagnosis, and Therapy," *J. Am. Med. Assoc.,* **285** [6] 785-95 (2001).

53. S. United States Public Health and G. S. G. U. States, *Bone Health and Osteoporosis: A Report of the Surgeon General*. University Press of the Pacific, 2004.

54. L. J. Melton, "The Prevalence of Osteoporosis: Gender and Racial Comparison," *Calcif. Tissue Int.,* **69** [4] 179-81 (2001).

55. E. Seeman, "Invited Review: Pathogenesis of Osteoporosis," *J. Appl. Physiol.,* **95** [5] 2142-51 (2003).

56. D. W. Dempster, E. Shane, W. Horbert, and R. Lindsay, "A Simple Method for Correlative Light and Scanning Electron Microscopy of Human Iliac Crest Bone Biopsies: Qualitative Observations in Normal and Osteoporotic Subjects," *J. Bone Miner. Res.,* **1** [1] 15-21 (1986).

57. O. Johnell and J. A. Kanis, "An Estimate of the Worldwide Prevalence and Disability Associated with Osteoporotic Fractures," *Osteoporos. Int.,* **17** [12] 1726-33 (2006).

58. S. Khosla, E. G. Lufkin, S. F. Hodgson, L. A. Fitzpatrick, and L. J. Melton, "Epidemiology and Clinical Features of Osteoporosis in Young Individuals," *Bone,* **15** [5] 551-5 (1994).

59. R. W. Chesney, "Vitamin D Deficiency and Rickets," *Rev. Endocr. Metab. Disord.,* **2** [2] 145-51 (2001).

60. J. M. Pettifor, "Rickets," *Calcif. Tissue Int.,* **70** [5] 398-9 (2002).

61. M. Moncrieff and T. O. Fadahunsi, "Congenital Rickets Due to Maternal Vitamin D Deficiency," *Arch. Dis. Child.,* **49** [10] 810-1 (1974).

62. M. K. Drezner, "Hypophosphatemic Rickets"; pp. 126-55 in Vol. 6, *Vitamin D and Rickets.* Karger Publishers, 2004.

63. E. S. Sirisl and G. D. Roodman, ". Paget's Disease of Bone," *ASBMR Primer on the Metabolic Bone Diseases and Disorders of Mineral Metabolism*, 335 (2009).

64. A. Morales-Piga, J. Rey-Rey, J. Corres-González, Í. S. Garc, and G. LÓPez-Abente, "Frequency and Characteristics of Familial Aggregation of Paget's Disease of Bone," *J. Bone Miner. Res.*, **10** [4] 663-70 (1995).

65. E. S. Siris, R. Ottman, E. Flaster, and J. L. Kelsey, "Familial Aggregation of Paget's Disease of Bone," *J. Bone Miner. Res.*, **6** [5] 495-500 (1991).

66. W. E. Friedrichs, S. V. Reddy, J. M. Bruder, T. Cundy, J. Cornish, F. R. Singer, and G. D. Roodman, "Sequence Analysis of Measles Virus Nucleocapsid Transcripts in Patients with Paget's Disease," *J. Bone Miner. Res.*, **17** [1] 145-51 (2002).

67. P. D. Costantino and C. D. Friedman, "Synthetic Bone Graft Substitutes," *Otolaryngol. Clin. North Am.*, **27** [5] 1037-74 (1994).

68. T. J. Cypher and J. P. Grossman, "Biological Principles of Bone Graft Healing," *The Journal of foot and ankle surgery*, **35** [5] 413-7 (1996).

69. W. R. Moore, S. E. Graves, and G. I. Bain, "Synthetic Bone Graft Substitutes," *ANZ J. Surg.*, **71** [6] 354-61 (2001).

70. L. T. Kurz, S. R. Garfin, and R. E. Booth Jr, "Harvesting Autogenous Iliac Bone Grafts: A Review of Complications and Techniques," *Spine (Phila Pa 1976)*, **14** [12] 1324-31 (1989).

71. J. C. Fernyhough, J. J. Schimandle, M. C. Weigel, C. C. Edwards, and A. M. Levine, "Chronic Donor Site Pain Complicating Bone Graft Harvesting from the Posterior Iliac Crest for Spinal Fusion," *Spine (Phila Pa 1976)*, **17** [12] 1474-80 (1992).

72. H. J. Mankin, M. C. Gebhardt, L. C. Jennings, D. S. Springfield, and W. W. Tomford, "Long-Term Results of Allograft Replacement in the Management of Bone Tumors," *Clin. Orthop. Relat. Res.*, **324** 86-97 (1996).

73. A. Sanan and S. J. Haines, "Repairing Holes in the Head: A History of Cranioplasty," *Neurosurgery*, **40** [3] 588-603 (1997).

74. J. Wilson, G. H. Pigott, F. J. Schoen, and L. L. Hench, "Toxicology and Biocompatibility of Bioglasses," *J. Biomed. Mater. Res., Part A*, **15** [6] 805-17 (1981).

75. J. Wilson and D. Nolletti, "Bonding of Soft Tissues to Bioglass®," *Handbook of bioactive ceramics*, **1** 283-302 (1990).

76. L. L. Hench, "Bioactive Ceramics," *Ann. N. Y. Acad. Sci.,* **523** [1] 54-71 (1988).

77. U. Gross, R. Kinne, H.-J. Schmitz, and V. Strunz, "The Response of Bone to Surface-Active Glasses Glass-Ceramics," *CRC critical reviews in biocompatibility,* **4** [2] 155-79 (1988).

78. L. L. Hench and A. E. Clark, "Adhesion to Bone," *Biocompat. Orthop. Implants,* **2** 129-70 (1982).

79. T. Kokubo, "Bioactive Glass Ceramics: Properties and Applications," *Biomaterials,* **12** [2] 155-63 (1991).

80. T. Kokubo and H. Takadama, "How Useful Is Sbf in Predicting in Vivo Bone Bioactivity," *Biomaterials,* **27** 2907-15 (2006).

81. W. Cao and L. L. Hench, "Bioactive Materials," *Ceram. Int.,* **22** [6] 493-507 (1996).

82. L. L. Hench, D. L. Wheeler, and D. C. Greenspan, "Molecular Control of Bioactivity in Sol-Gel Glasses," *J. Sol-Gel Sci. Technol.,* **13** [1] 245-50 (1998).

83. H. Takadama, H.-M. Kim, T. Kokubo, and T. Nakamura, "Xps Study of the Process of Apatite Formation on Bioactive Ti-6al-4v Alloy in Simulated Body Fluid," *Sci. Technol. Adv. Mater.,* **2** 389-96 (2001).

84. D. Arcos, D. C. Greenspan, and M. Vallet-Regí, "A New Quantitative Method to Evaluate the in Vitro Bioactivity of Melt and Sol-Gel-Derived Silicate Glasses," *J. Biomed. Mater. Res., Part A,* **65** [3] 344-51 (2003).

85. R. Z. Legfros, T. Sakae, C. Bautista, M. Retino, and J. P. LeGeros, "Magnesium and Carbonate in Enamel and Synthetic Apatites," *Adv. Dent. Res.,* **10** [2] 225-31 (1996).

86. H. Takadama, H.-M. Kim, T. Kokubo, and T. Nakamura, "Mechanism of Biomineralization of Apatite on a Sodium Silicate Glass: Tem− Edx Study in Vitro," *Chem. Mater.,* **13** [3] 1108-13 (2001).

87. J. D. Santos, L. J. Jha, and F. J. Monteiro, "Surface Modifications of Glass-Reinforced Hydroxyapatite Composites," *Biomaterials,* **16** [7] 521-6 (1995).

88. J. D. Santos, L. J. Jha, and F. J. Monteiro, "In Vitro Calcium Phosphate Formation on Sio2-Na2o-Cao-P2o5 Glass Reinforced Hydroxyapatite Composite: A Study by Xps Analysis," *J. Mater. Sci. Mater. Med.,* **7** [3] 181-5 (1996).

89. Z.-h. Zhou, J.-m. Ruan, Z.-c. Zhou, and X.-j. Shen, "Bioactivity of Bioresorbable Composite Based on Bioactive Glass and Poly-L-Lactide," *Trans. Nonferrous Met. Soc. China,* **17** [2] 394-9 (2007).

90. H. H. Lu, S. R. Pollack, and P. Ducheyne, "45s5 Bioactive Glass Surface Charge Variations and the Formation of a Surface Calcium Phosphate Layer in a Solution Containing Fibronectin," *J. Biomed. Mater. Res.,* **54** [3] 454-61 (2001).

91. I. D. Xynos, M. V. J. Hukkanen, J. J. Batten, L. D. Buttery, L. L. Hench, and J. M. Polak, "Bioglass® 45s5 Stimulates Osteoblast Turnover and Enhances Bone Formation in Vitro: Implications and Applications for Bone Tissue Engineering," *Calcif. Tissue Int.,* **67** [4] 321-9 (2000).

92. S. K. Ghosh, S. K. Nandi, B. Kundu, S. Datta, D. K. De, S. K. Roy, and D. Basu, "In Vivo Response of Porous Hydroxyapatite and B-Tricalcium Phosphate Prepared by Aqueous Solution Combustion Method and Comparison with Bioglass Scaffolds," *J. Biomed. Mater. Res., Part B,* **86** [1] 217-27 (2008).

93. Q. Z. Chen, I. D. Thompson, and A. R. Boccaccini, "45s5 Bioglass®-Derived Glass–Ceramic Scaffolds for Bone Tissue Engineering," *Biomaterials,* **27** [11] 2414-25 (2006).

94. S. Haimi, G. Gorianc, L. Moimas, B. Lindroos, H. Huhtala, S. Räty, H. Kuokkanen, G. K. Sándor, C. Schmid, and S. Miettinen, "Characterization of Zinc-Releasing Three-Dimensional Bioactive Glass Scaffolds and Their Effect on Human Adipose Stem Cell Proliferation and Osteogenic Differentiation," *Acta Biomaterialia,* **5** [8] 3122-31 (2009).

95. J. Temenoff, L. Lu, and A. Mikos, "Bone Tissue Engineering Using Synthetic Biodegradable Polymer Scaffolds," *Bone engineering,* 454 (2000).

96. S. P. Bruder and A. I. Caplan, "Bone Regeneration through Cellular Engineering," *Principles of tissue engineering,* **2** 683-96 (2000).

97. J. Jones and A. Boccaccini, "Cellular Ceramics in Biomedical Applications: Tissue Engineering," *Cellular Ceramics: Structure, Manufacturing, Processing and Applications,* 550-73 (2005).

98. L.-C. Gerhardt and A. R. Boccaccini, "Bioactive Glass and Glass-Ceramic Scaffolds for Bone Tissue Engineering," *Materials,* **3** [7] 3867-910 (2010).

99. K. Rezwan, Q. Chen, J. Blaker, and A. R. Boccaccini, "Biodegradable and Bioactive Porous Polymer/Inorganic Composite Scaffolds for Bone Tissue Engineering," *Biomaterials,* **27** [18] 3413-31 (2006).

100. S. Yang, K.-F. Leong, Z. Du, and C.-K. Chua, "The Design of Scaffolds for Use in Tissue Engineering. Part I. Traditional Factors," *Tissue Eng.,* **7** [6] 679-89 (2001).

101. V. Karageorgiou and D. Kaplan, "Porosity of 3d Biomaterial Scaffolds and Osteogenesis," *Biomaterials,* **26** [27] 5474-91 (2005).

102. Y. Tabata, "Biomaterial Technology for Tissue Engineering Applications," *J. R. Soc., Interface,* **6** [Suppl 3] S311-S24 (2009).

103. H. Oonishi, S. Kushitani, E. Yasukawa, H. Iwaki, L. L. Hench, J. Wilson, E. Tsuji, and T. Sugihara, "Particulate Bioglass Compared with Hydroxyapatite as a Bone Graft Substitute," *Clin. Orthop. Relat. Res.,* **334** 316-25 (1997).

104. L. L. Hench and H. Paschall, "Direct Chemical Bond of Bioactive Glass-Ceramic Materials to Bone and Muscle," *J. Biomed. Mater. Res., Part A,* **7** [3] 25-42 (1973).

105. L. Hench and H. Paschall, "Histochemical Responses at a Biomaterial's Interface," *J. Biomed. Mater. Res.,* **8** [3] 49-64 (1974).

106. A. Clark and L. Hench, "Calcium Phosphate Formation on Sol-Gel Derived Bioactive Glasses," *J. Biomed. Mater. Res.,* **28** 693-8 (1994).

107. L. L. Hench, "Sol-Gel Materials for Bioceramic Applications," *Curr. Opin. Solid State Mater. Sci.,* **2** [5] 604-10 (1997).

108. L. L. Hench and J. Wilson, "Surface-Active Biomaterials," *Science,* **226** 630-6 (1984).

109. A. Gatti, G. Valdre, and Ö. Andersson, "Analysis of the in Vivo Reactions of a Bioactive Glass in Soft and Hard Tissue," *Biomaterials,* **15** [3] 208-12 (1994).

110. T. Livingston, P. Ducheyne, and J. Garino, "In Vivo Evaluation of a Bioactive Scaffold for Bone Tissue Engineering," *J. Biomed. Mater. Res.,* **62** [1] 1-13 (2002).

111. E. Effah Kaufmann, P. Ducheyne, and I. Shapiro, "Evaluation of Osteoblast Response to Porous Bioactive Glass (45s5) Substrates by Rt-Pcr Analysis," *Tissue Eng.,* **6** [1] 19-28 (2000).

112. H. Yuan, J. D. de Bruijn, X. Zhang, C. A. van Blitterswijk, and K. de Groot, "Bone Induction by Porous Glass Ceramic Made from Bioglass®(45s5)," *J. Biomed. Mater. Res., Part A,* **58** [3] 270-6 (2001).

113. J. R. Jones and L. L. Hench, "Factors Affecting the Structure and Properties of Bioactive Foam Scaffolds for Tissue Engineering," *J. Biomed. Mater. Res., Part B,* **68** [1] 36-44 (2004).

114. D. C. Tancred, A. J. Carr, and B. A. O. McCormack, "The Sintering and Mechanical Behavior of Hydroxyapatite with Bioglass Additions," *J. Mater. Sci. Mater. Med.,* **12** [1] 81-93 (2001).

115. Q. Fu, M. N. Rahaman, B. S. Bal, and R. F. Brown, "Preparation and in Vitro Evaluation of Bioactive Glass (13–93) Scaffolds with Oriented Microstructures for Repair and Regeneration of Load-Bearing Bones," *J. Biomed. Mater. Res., Part A,* **93** [4] 1380-90 (2010).

116. J. Kanczler and R. Oreffo, "Osteogenesis and Angiogenesis: The Potential for Engineering Bone," *Eur Cell Mater,* **15** [2] 100-14 (2008).

117. F. Baino, E. Verné, and C. Vitale-Brovarone, "3-D High-Strength Glass–Ceramic Scaffolds Containing Fluoroapatite for Load-Bearing Bone Portions Replacement," *Mater. Sci. Eng., C,* **29** [6] 2055-62 (2009).

118. C. Hernandez, G. Beaupre, T. Keller, and D. Carter, "The Influence of Bone Volume Fraction and Ash Fraction on Bone Strength and Modulus," *Bone,* **29** [1] 74-8 (2001).

119. D. Clupper and L. Hench, "Crystallization Kinetics of Tape Cast Bioactive Glass 45s5," *J. Non-Cryst. Solids,* **318** [1] 43-8 (2003).

120. I. Ochoa, J. A. Sanz-Herrera, J. M. García-Aznar, M. Doblaré, D. M. Yunos, and A. R. Boccaccini, "Permeability Evaluation of 45s5 Bioglass®-Based Scaffolds for Bone Tissue Engineering," *J. Biomech.,* **42** [3] 257-60 (2009).

121. C. Vitale-Brovarone, E. Verne, M. Bosetti, P. Appendino, and M. Cannas, "Microstructural and in Vitro Characterization of Sio2-Na2o-Cao-Mgo Glass-Ceramic Bioactive Scaffolds for Bone Substitutes," *J. Mater. Sci. Mater. Med.,* **16** [10] 909-17 (2005).

122. L. Moimas, M. Biasotto, R. Di Lenarda, A. Olivo, and C. Schmid, "Rabbit Pilot Study on the Resorbability of Three-Dimensional Bioactive Glass Fibre Scaffolds," *Acta biomaterialia,* **2** [2] 191-9 (2006).

123. Q. Fu, M. N. Rahaman, B. S. Bal, W. Huang, and D. E. Day, "Preparation and Bioactive Characteristics of a Porous 13–93 Glass, and Fabrication into the Articulating Surface of a Proximal Tibia," *J. Biomed. Mater. Res., Part A,* **82** [1] 222-9 (2007).

124. S. Deville, E. Saiz, R. K. Nalla, and A. P. Tomsia, "Freezing as a Path to Build Complex Composites," *Science,* **311** [5760] 515-8 (2006).

125. V. Cannillo, F. Chiellini, P. Fabbri, and A. Sola, "Production of Bioglass® 45s5–Polycaprolactone Composite Scaffolds Via Salt-Leaching," *Compos. Struct.,* **92** [8] 1823-32 (2010).

126. L. Bertolla, I. Dlouhý, and A. Boccaccini, "Preparation and Characterization of Bioglass®-Based Scaffolds Reinforced by Poly-Vinyl Alcohol/Microfibrillated Cellulose Composite Coating," *J. Eur. Ceram. Soc.,* **34** [14] 3379-87 (2014).

127. W. Li, P. Nooeaid, J. A. Roether, D. W. Schubert, and A. R. Boccaccini, "Preparation and Characterization of Vancomycin Releasing Phbv Coated 45s5 Bioglass®-Based Glass–Ceramic Scaffolds for Bone Tissue Engineering," *J. Eur. Ceram. Soc.,* **34** [2] 505-14 (2014).

128. P. Fabbri, L. Valentini, J. Hum, R. Detsch, and A. R. Boccaccini, "45s5 Bioglass®-Derived Scaffolds Coated with Organic–Inorganic Hybrids Containing Graphene," *Mater. Sci. Eng., C,* **33** [7] 3592-600 (2013).

129. M. Peter, N. Binulal, S. Nair, N. Selvamurugan, H. Tamura, and R. Jayakumar, "Novel Biodegradable Chitosan–Gelatin/Nano-Bioactive Glass Ceramic Composite Scaffolds for Alveolar Bone Tissue Engineering," *Chem. Eng. J.,* **158** [2] 353-61 (2010).

130. D. Arcos, D. Greenspan, and M. Vallet-Regi, "Influence of the Stabilization Temperature on Textural and Structural Features and Ion Release in Sio2− Cao− P2o5 Sol− Gel Glasses," *Chem. Mater.,* **14** [4] 1515-22 (2002).

131. T. Waltimo, T. Brunner, M. Vollenweider, W. Stark, and M. Zehnder, "Antimicrobial Effect of Nanometric Bioactive Glass 45s5," *J. Dent. Res.,* **86** [8] 754-7 (2007).

132. M. Vogel, C. Voigt, U. M. Gross, and C. M. Müller-Mai, "In Vivo Comparison of Bioactive Glass Particles in Rabbits," *Biomaterials,* **22** [4] 357-62 (2001).

133. A. W. Wren, F. R. Laffir, A. Kidari, and M. R. Towler, "The Structural Role of Titanium in Ca-Sr-Zn-Si/Ti Glasses for Medical Applications.," *J. Non-Cryst. Solids,* **Submitted Manuscript** [357] 1021-6 (2011).

134. A. Bachar, C. Mercier, A. Tricoteaux, A. Leriche, C. Follet, M. Saadi, and S. Hampshire, "Effects of Addition of Nitrogen on Bioglass Properties and Structure," *J. Non-Cryst. Solids,* **358** [3] 693-701 (2012).

135. M. N. Rahaman, D. E. Day, B. S. Bal, Q. Fu, S. B. Jung, L. F. Bonewald, and A. P. Tomsia, "Bioactive Glass in Tissue Engineering," *Acta biomaterialia,* **7** [6] 2355-73 (2011).

136. V. Shrikhande, "Nmr Studies on Lead Silicate Glasses Containing Alkali Metal Oxides"; p. 258 in Vol. 41. Universities Press,

137. M. C. Davis, K. J. Sanders, P. J. Grandinetti, S. J. Gaudio, and S. Sen, "Structural Investigations of Magnesium Silicate Glasses by 29 Si 2d Magic-Angle Flipping Nmr," *J. Non-Cryst. Solids,* **357** [15] 2787-95 (2011).

138. A. Gaddam, H. R. Fernandes, D. U. Tulyaganov, M. J. Pascual, and J. M. Ferreira, "Role of Manganese on the Structure, Crystallization and Sintering of Non-Stoichiometric Lithium Disilicate Glasses," *RSC Advances,* **4** [26] 13581-92 (2014).

139. R. A. Martin, R. M. Moss, N. J. Lakhkar, J. C. Knowles, G. J. Cuello, M. E. Smith, J. V. Hanna, and R. J. Newport, "Structural Characterization of Titanium-Doped Bioglass Using Isotopic Substitution Neutron Diffraction," *Phys. Chem. Chem. Phys.,* **14** [45] 15807-15 (2012).

140. A. Hoppe, R. Meszaros, C. Stähli, S. Romeis, J. Schmidt, W. Peukert, B. Marelli, S. N. Nazhat, L. Wondraczek, and J. Lao, "In Vitro Reactivity of Cu Doped 45s5 Bioglass® Derived Scaffolds for Bone Tissue Engineering," *J. Mater. chem. B,* **1** [41] 5659-74 (2013).

141. L. Cormier, O. Dargaud, N. Menguy, G. S. Henderson, M. Guignard, N. Trcera, and B. Watts, "Investigation of the Role of Nucleating Agents in Mgo− Sio2− Al2o3− Sio2− Tio2 Glasses and Glass-Ceramics: A Xanes Study at the Ti K-and L2, 3-Edges," *Cryst. Growth Des.,* **11** [1] 311-9 (2010).

142. V. Rajendran, A. V. G. Devi, M. Azooz, and F. H. El-Batal, "Physicochemical Studies of Phosphate Based P 2 O 5–Na 2 O–Cao–Tio 2 Glasses for Biomedical Applications," *J. Non-Cryst. Solids,* **353** [1] 77-84 (2007).

143. O. Peitl Filho, G. P. Latorre, and L. Hench, "Effect of Crystallization on Apatite-Layer Formation of Bioactive Glass 45%," *J Biomed Mater Res,* **30** 509-14 (1996).

144. O. Peitl, E. D. Zanotto, and L. L. Hench, "Highly Bioactive P 2 O 5–Na 2 O–Cao–Sio 2 Glass-Ceramics," *J. Non-Cryst. Solids,* **292** [1] 115-26 (2001).

145. D. Clupper, J. Mecholsky, G. LaTorre, and D. Greenspan, "Sintering Temperature Effects on the in Vitro Bioactive Response of Tape Cast and Sintered Bioactive Glass-Ceramic in Tris Buffer," *J. Biomed. Mater. Res., Part A,* **57** [4] 532-40 (2001).

146. D. C. Clupper, J. J. Mecholsky, G. P. LaTorre, and D. C. Greenspan, "Bioactivity of Tape Cast and Sintered Bioactive Glass-Ceramic in Simulated Body Fluid," *Biomaterials,* **23** [12] 2599-606 (2002).

147. W. Lai, J. Garino, and P. Ducheyne, "Silicon Excretion from Bioactive Glass Implanted in Rabbit Bone," *Biomaterials,* **23** [1] 213-7 (2002).

148. N. Saffarian Tousi, M. F. Velten, T. J. Bishop, K. K. Leong, N. S. Barkhordar, G. W. Marshall, P. M. Loomer, P. B. Aswath, and V. G. Varanasi, Vol. 33, p. 2757-65.

149. F. Talo, M. Senila, T. Frentiu, and S. Simon, "Effect of Titanium Ions on the Ion Release Rate and Uptake at the Interface of Silica Based Xerogels with Simulated Body Fluid " *Corrs. Sci.,* **72** 41-6 (2013).

150. Q.-Z. Chen, Y. Li, L.-Y. Jin, J. M. W. Quinn, and P. A. Komesaroff, "A New Sol–Gel Process for Producing Na 2 O-Containing Bioactive Glass Ceramics," *Acta Biomaterialia,* **6** [10] 4143-53 (2010).

151. S. Kashyap, K. Griep, and J. A. Nychka, "Crystallization Kinetics, Mineralization and Crack Propagation in Partially Crystallized Bioactive Glass 45s5," *Mater. Sci. Eng., C,* **31** [4] 762-9 (2011).